



SCHOOL of
GRADUATE STUDIES
EAST TENNESSEE STATE UNIVERSITY

East Tennessee State University
Digital Commons @ East
Tennessee State University

Electronic Theses and Dissertations

Student Works


5-2019

Development of Granulated Adsorbent for Clean-up of Water contaminated by Cesium

Esther Alorkpa

East Tennessee State University

Follow this and additional works at: <https://dc.etsu.edu/etd>

 Part of the [Analytical Chemistry Commons](#), [Environmental Chemistry Commons](#), [Inorganic Chemistry Commons](#), and the [Materials Chemistry Commons](#)

Recommended Citation

Alorkpa, Esther, "Development of Granulated Adsorbent for Clean-up of Water contaminated by Cesium" (2019). *Electronic Theses and Dissertations*. Paper 3558. <https://dc.etsu.edu/etd/3558>

This Thesis - Open Access is brought to you for free and open access by the Student Works at Digital Commons @ East Tennessee State University. It has been accepted for inclusion in Electronic Theses and Dissertations by an authorized administrator of Digital Commons @ East Tennessee State University. For more information, please contact digilib@etsu.edu.

Development of Granulated Adsorbent for Clean-up of Water Contaminated by Cesium

A thesis

presented to

the faculty of the Department of Chemistry

East Tennessee State University

In partial fulfillment

of the requirements for the degree

Master of Science in Chemistry

by

Esther Jemma Alorkpa

May 2019

Dr. Aleksey Vasiliev, Chair

Dr. Marina Roginskaya

Dr. Greg Bishop

Keywords: Tetraethylorthosilicate, aluminium oxide, covalent bonding, Kegging units,
granulation, contaminated water

ABSTRACT

Development of Granulated Adsorbent for Clean-up of Water contaminated by Cesium

by

Esther Jemima Alorkpa

A study was conducted on sol-gel synthesis of an adsorbent (phosphotungstic acid embedded in silica gel, H-PTA/SiO₂) of radioactive cesium. A novelty of this work is covalent bonding of PTA to the surface of solid support that prevents leaching from the surface of the material. The sample was granulated with a binder, aluminium oxide (γ -Al₂O₃). Solid-state NMR and FT-IR spectroscopy were used to confirm the presence of Keggin units of PTA in the bound materials. Thermal analysis of H-PTA/SiO₂ - γ -Al₂O₃ (50 %) showed that the water content in the bound material was appreciably lower than in the pure adsorbent. Quantitative determination of surface acidity of porous materials is an important analytical problem in characterization of the adsorbents. This problem was solved by reversed titration after saturation of the materials by anhydrous solution of pyridine. Batch and column adsorption tests showed that the adsorbent demonstrated high adsorption capacities towards cesium.

DEDICATION

This work is dedicated to my late Mum, Beatrice and Dad, Christoph, my siblings, Sylvia Alorkpa, Daniel Alorkpa, Millicent Agbodza, Naomi Agbodza, and my beloved Charles Agbavor.

ACKNOWLEDGEMENTS

I would like to appreciate Dr. Vasiliev for being helpful throughout this research.

I also want to appreciate Dr. Roginskaya for her helping in reviewing my thesis and answering all questions and always helping me anytime I need help.

Thank you, Dr. Bishop, for helping me with questions regarding analytical instrumentations and in reviewing my thesis.

My final appreciation to Dr. Mohseni for his help in this research.

NATO's Emerging Security Challenges Division in the framework of the Science for Peace and Security Programme (grant SfP 984639) sponsored this research.

TABLE OF CONTENTS

	Page
ABSTRACT.....	2
DEDICATION.....	3
ACKNOWLEDGEMENTS.....	4
LIST OF FIGURES.....	8
LIST OF ABBREVIATIONS.....	9
Chapter	
1. INTRODUCTION.....	10
Origin, Properties and Chemistry of Cesium.....	10
Distribution of Cesium into the Environment and its Impacts.....	11
Contamination of Land and Water from Nuclear Accidents.....	12
Chernobyl Accident.....	12
Fukushima Daichi Nuclear Power Plant (FDNPP) Accident.....	13
Adsorption of Cesium.....	15
Heteropolyacids.....	19
Immobilization of HPAs.....	21
Impregnation Method.....	21
Covalent Immobilization.....	21
Research Objectives.....	22
2. EXPERIMENTAL / METHODOLOGY.....	23
Materials Used.....	23
Synthesis and Granulation.....	23
Sol-gel Method.....	23
Granulation Process.....	24

Structural and Instrumental Characterization	24
X-ray Fluorescence (XRF) Study	24
Elemental Analysis	24
Fourier-Transform Infrared (FT-IR) Spectroscopy	25
Nuclear Magnetic Resonance (NMR) Spectroscopy	25
Surface Acidity	25
Scanning Electron Microscopy (SEM) and Transmission Electron Microscopy (TEM)	26
Particle Size Distribution	26
X-ray Diffraction (XRD)	26
Porosity	26
Thermogravimetric Analysis (TGA) and Differential Scanning Calorimetry (DSC)	27
Adsorption Studies	27
Batch Tests	27
Column Tests	27
3. RESULTS AND DISCUSSION	29
Synthesis and Granulation	29
Sol-gel Synthesis and Ion-exchange	29
Granulation	29
Structural and Instrumental Characterization	29
XRF Study	29
FT-IR Spectroscopy	29
NMR Spectroscopy	30
Surface Acidity	31

SEM and TEM.....	31
Particle Size Distribution.....	33
XRD Study.....	34
Porosity.....	34
Thermal Analysis.....	36
Adsorption Studies	38
Batch Tests.....	38
Column Tests.....	38
Discussion.....	40
Conclusion.....	44
REFERENCES	45
VITA.....	53

LIST OF FIGURES

Figure	Page
1. Diagram of ^{137}Cs radioactive decay	11
2. Contamination of Europe after Chernobyl accident	14
3. Radiation in the environment around Fukushima.....	15
4. O-benzo-p-xylyl-22-crown-6-ether.....	16
5. Structures of Calix [4] arenes R14.....	17
6. Keggin structures of $\text{H}_3\text{PW}_{12}\text{O}_{40}$	21
7. An outline of the reaction of HPA with pyridine	26
8. FT-IR spectra of 1 , 2 , 1-2 (10 %), 1-2 (30 %) and 1-2 (50 %).....	31
9. ^{31}P and ^{27}Al NMR spectra of 1-2 (50 %)	31
10. (a) SEM images of 1 , and 1-2 (50 %), and (b) TEM images of 1-2 (50 %)	32
11. (a) Particle size distribution of 1 , 2 , and 1-2 (50 %), (b) Particle size distribution of 1-2 (50 %) before (a) and after (b) adsorption of cesium	33
12. XRD patterns of 1-2 (50 %).....	34
13. (a) N_2 adsorption isotherm of 1 , and 2 (b) N_2 adsorption isotherm of 1-2 (10 %), 1-2 (30 %), and 1-2 (50 %) (c) N_2 adsorption/desorption isotherms of 1-2 (50 %) before (a) and after (b) adsorption of cesium.....	35
14. Pore size distribution of adsorbents and bound materials (a)Pore diameter of 1 , 2 (b) Pore diameter of 1-2 (10 %, 30 %,50 %) (c) Pore half width of before (a) and after (b) adsorption of Cs	37
15. DSC and TGA curves of 1-2 (50 %).....	38
16. Adsorption of Cs from CsCl solutions (20, 50, and 100 mg/L) on bound materials ...	39
17. Graph of adsorption of cesium on 1-2 (50 %) from CsCl solution (0.15 mmol/L) and its mixtures with NaCl and KCl (0.15-1.5 mmol/L)	40

LIST OF ABBREVIATIONS

AAS	Atomic Absorption Spectroscopy
BET	Brunauer-Emmett-Teller Theory
Cs-PTA/SiO ₂	Cesium-Exchanged Phosphotungstic Acid/Silica gel
CuFC	Copper Ferrocyanide
DFT	Density Functional Theory
DSC	Differential Scanning Calorimetry
FDNPP	Fukushima Daichi Nuclear Power Plant
FT-IR	Fourier Transform Infrared Spectroscopy
HPA	Heteropolyacid
H-PTA/SiO ₂	Phosphotungstic Acid Embedded in Silica Gel
LTBT	Limited Test Ban Treaty
NMR	Nuclear Magnetic Resonance
OBPX22C6	O-benzo-p-xylyl-22-crown-6-ether
PAN	Polyacrylonitrile
PDI	Polydispersity index
PTA	Phosphotungstic Acid
TEM	Transmission Electron Microscopy
TEOS	Tetraethyl orthosilicate
TGA	Thermogravimetric Analysis
XRD	X-Ray Diffraction
XRF	X-Ray Fluorescence

CHAPTER 1

INTRODUCTION

Origin, Properties and Chemistry of Cesium

Cesium was discovered by Bunsen and Kirchhoff in a Bavarian mineral spring. Cs occurs as a pollutant in the USA and Africa which are recognized as the major geographical sources of cesium. ^{133}Cs is stable and it is known as the scarcest of alkali metals with minute economic value. Studies show that there are over twenty isotopes of cesium ranging from ^{123}Cs to ^{144}Cs excluding ^{124}Cs . All isotopes of cesium except for ^{133}Cs are radioactive with either short or long half-lives. Among the isotopes of cesium, ^{137}Cs had been reported of 30.2 years of half-life. ^{134}Cs has a half-life of approximately 2.07 years. ^{135}Cs had also been reported of 2.3 million years of half-life.²

^{134}Cs decays via beta emission and produces one beta particle per each transformation. Research show that the mean energy produced from the beta emission of ^{134}Cs decay is 0.157 MeV and the mean energy produced from the emission of gamma rays is 0.698 MeV. ^{135}Cs undergoes beta decay and produces one beta particle per transformation with a mean energy of 0.188 MeV.³ During the radioactive decay of ^{137}Cs , 92% of beta particles are emitted via excited state producing 89% of gamma radiation. However, 8% of the beta particles are emitted directly producing stable ^{137}Ba as shown in Figure 1 below.⁴

Cesium is very useful in brachytherapy for treating cancer. In addition, it is an excellent source of radiation in radiotherapy and disinfection of medical instruments.⁵ Also, it is less expensive and has demonstrated good characteristics making it a very useful substitute for radium in treatment of malignant disease.⁶ Over the years, Cs attracted little interest until the origination of nuclear power.¹

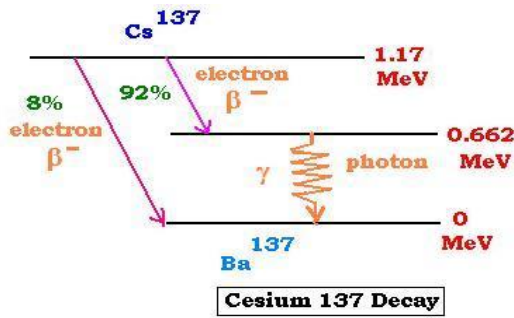


Figure 1: Diagram of ^{137}Cs radioactive decay.⁴

Distribution of Cesium into the Environment and its Impacts

Research shows that the spreading of radioactive cesium into the environment is due to the release of ^{137}Cs and ^{134}Cs .⁷ ^{137}Cs is released into the environment by three ways. Nuclear weapons testing is one of the routes that led to the pollution of the atmosphere. Developed countries such as United States, the United Kingdom, Russia, France, and China were leading this radioactive contamination with massive nuclear tests in the atmosphere. In 1963 there was a breakthrough with the passing of the Limited Test Ban Treaty (LTBT), banning the testing of nuclear weapons in all global environments, except for underground.⁸ Though this treaty was passed banning all nuclear tests in the atmosphere, France and China continued nuclear testing in the atmosphere.

The nuclear-armed states, represented by India, South Africa, Pakistan, North Korea, and Israel was the second category that developed after this period and they continued testing nuclear weapons underground.⁹

With respect to all the nuclear tests carried-out in the atmosphere from 1945-1963, the USA and Russia were responsible for 82 % of all these tests. Between 1951 and 1992, nuclear tests totalled an explosive yield of approximately 530 Megatonnes, of which 83 % were due to the atmospheric nuclear tests carried out.¹⁰

The discharge of waste effluents generated from nuclear fuel-reprocessing plants and nuclear reactors led to the second route. The last route is through the accidental leaks of

radioisotopes from nuclear power plants and this route is an environmental concern since the radionuclides speedily disperse into the environment.¹

The trace of radioactive substances in water bodies is mainly due to radionuclides washing off from the water-catchment areas. Radionuclides are rapidly redistributed and accumulated in aquatic plants, fish and soil sediments.¹¹ The contamination of biological systems are due to the radiation exposure of aquatic organisms and humans connected by food-chains within the hydrosphere. The migration of ¹³⁷Cs into water bodies led to contamination and damaged many aquatic habitants. Consequently, humans are at high risk since fish is a major source of food to humans.¹²

Cesium enters the human body and it spreads throughout the body at higher concentrations into the muscle tissues. Essentially, all cesium that is ingested is absorbed into the bloodstream through the intestines. However, cesium is excreted from the body quickly. The accumulation of cesium into the body poses health hazards from both gamma and beta radiation. This has become a concern due to the increased likelihood for causing cancer.¹³

The radioactivity emitted by cesium shows dietary exposure of adults at certain locales in Japan.¹⁴ After nuclear accidents, there was large exposure of radioactive ¹³⁷Cs and this became a serious concern due to health problems associated with it.¹⁵

Contamination of Land and Water from Nuclear Accidents

Chernobyl Accident

The Chernobyl nuclear power plant accident occurred on April 26, 1986. Studies show that its surroundings were contaminated with radionuclides. This accident affected the atomic power station in Ukraine and resulted in the spread of significant amounts of radionuclides. A complete breakdown of the nuclear reactor took place, and about 150 to 200 million curies of radioactive substances were distributed into the atmosphere during the first week of the accident.¹⁶

The Chernobyl accident affected people about hundreds of kilometres away from the atomic power station resulting into several cancerous conditions with higher incidence of tumour type cancers. Thyroid tumours were the largest spread of cancers in the affected population.¹⁷ The flood plain of Pripyat River was contaminated by ¹³⁴Cs and ¹³⁷Cs due to its proximity to the nuclear plant.¹⁸ Several studies investigated Cs pollution of soil and water surfaces and they provided estimates of dissolved ¹³⁷Cs in Chernobyl.¹⁹

About 450 different radioactive materials were distributed into the atmosphere affecting Ukraine, Belarus and Russia. The radioactive cloud travelled to the Baltic states, Scandinavia, Europe and radioactive materials were even detected over North America. Millions of people were exposed to high quantities of radioisotopes with millions of children suffering from thyroidal conditions.²⁰

After the deposition of radiocesium from the nuclear accident, it led to the distribution of radionuclides in alpine which affected alpine pastures that were used extensively in agricultural land for milk production.²¹ The aquatic system was reported to be contaminated after the Chernobyl accident. Sequentially, aquatic systems became the source of radionuclides due to the deposition of ¹³⁷Cs and ⁹⁰Sr in the terrestrial areas which lead to the transportation of higher number of radionuclides transported to groundwater, lakes, and rivers.²² Subsequently, the discharge of nuclear fuel from Chernobyl nuclear accident led to the transportation of ¹³⁷Cs into the Siberian Arctic. Several studies show that the Barents Sea, Pechora Sea, Kara Sea, Ob River, and the Yenisey River were largely polluted by ¹³⁷Cs.²³ Figure 2 below shows the effect of Chernobyl nuclear accident.

Fukushima Daichi Nuclear Power Plant (FDNPP) Accident

This nuclear accident occurred on March 11, 2011 in Japan. This disaster was triggered by the tsunami following the Tōhoku earthquake and affected several nuclear plants in Japan concurrently, thereby causing drastic contamination in Fukushima.

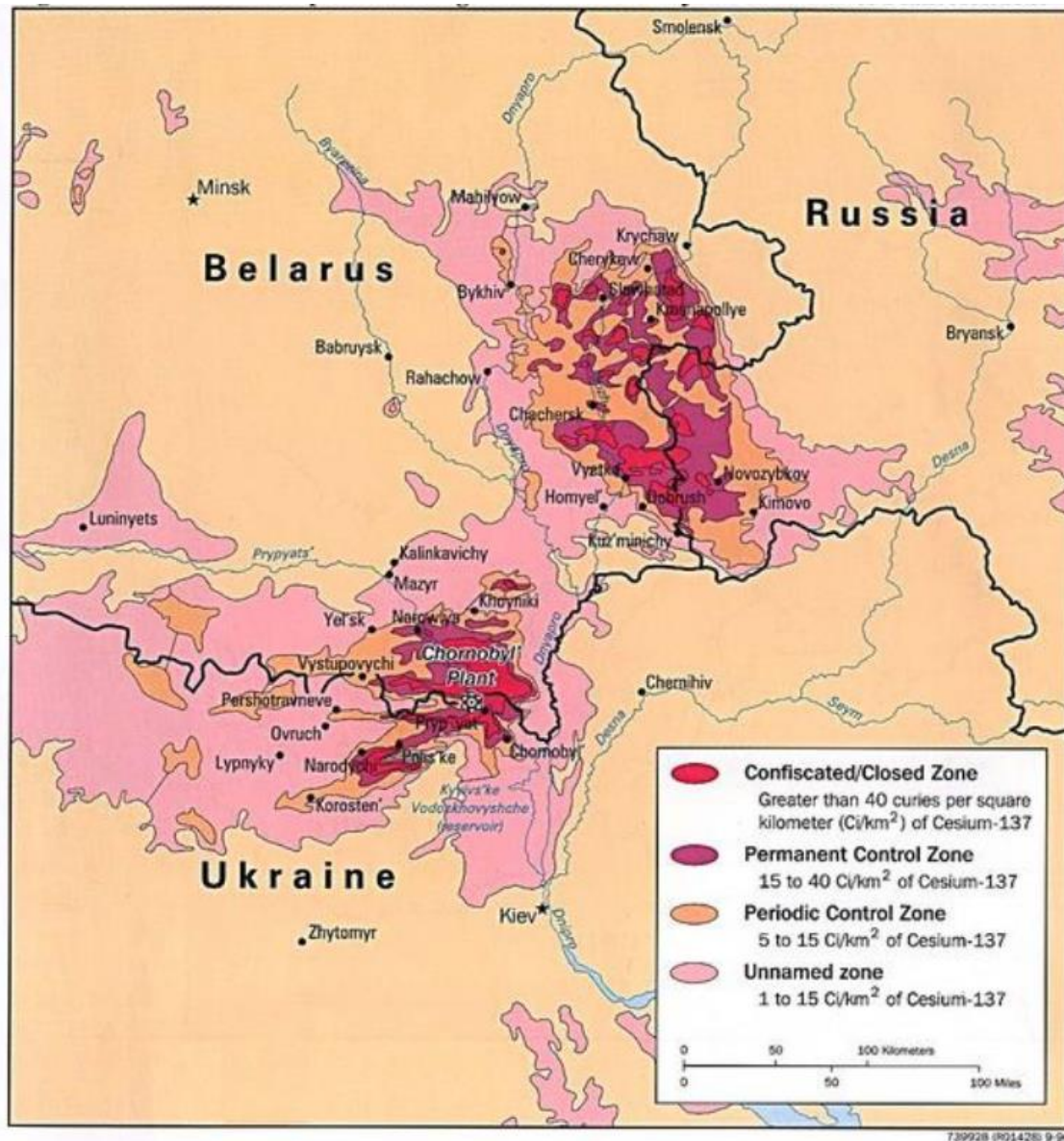


Figure 2: Radiation contamination after Chernobyl disaster

(<http://chm.gmu.edu/1989/items/show/173> accessed April 10, 2019, 11:44 am)

The nuclear accident led to rapid transportation and distribution of radionuclides such as ¹³⁷Cs and ¹³⁴Cs into river sediments which in turn affected potable water.²⁴ After the Fukushima disaster, most research conducted show that drinking waters around Fukushima were heavily contaminated with large amount of radioactive cesium.²⁵ Thus, radionuclides were distributed into the atmosphere because of the nuclear accident.²⁶

The release of ¹³¹I and ¹³⁷Cs led to severe atmospheric pollution.²⁷ Consequently, the release of radioactive ¹³⁷Cs substances into the environment led to skin injuries and caused

acute radiation syndrome.²⁸ Figure 3 below shows contamination of surroundings around Fukushima.

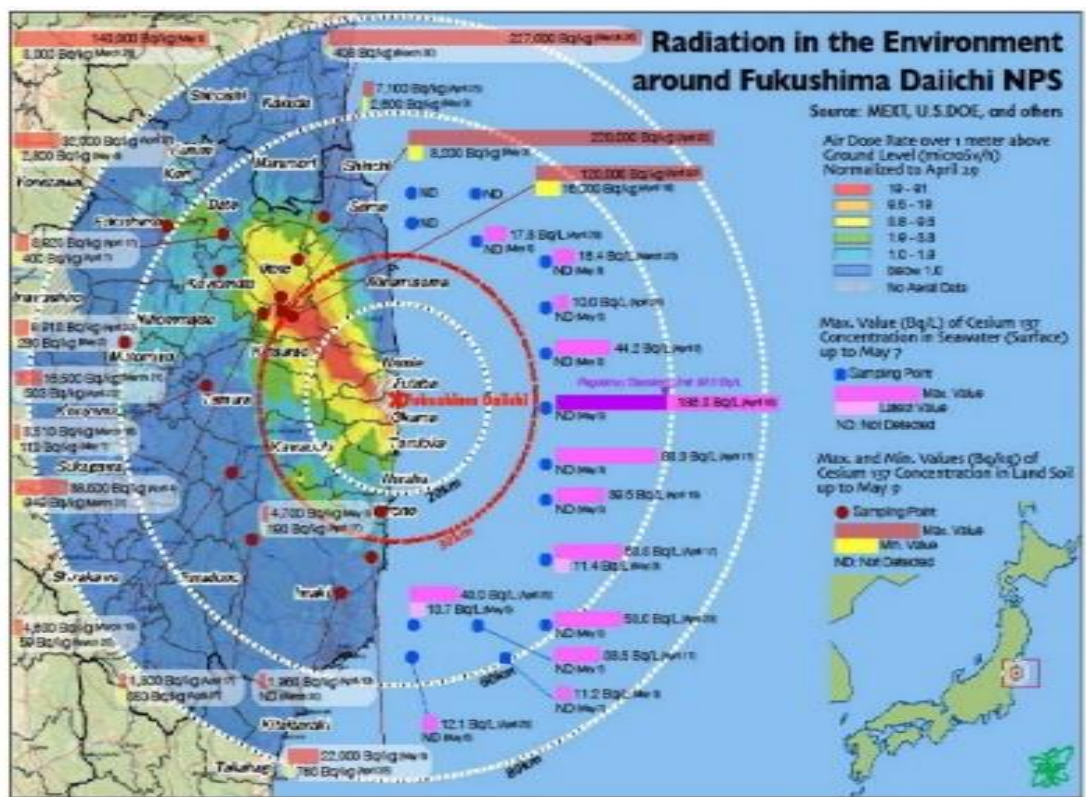


Figure 3: Radiation in the environment around Fukushima (US DOE)

Adsorption of Cesium

There have been several techniques to remove cesium from wastewater to prevent contamination. One such novel method is the application of macrocyclic ligand, o-benzo-p-xylyl-22-crown-6-ether (OBPX22C6) as shown in Figure 4 and it is very useful in the adsorption of cesium from wastewater. There is a high propensity of the π electron of this crown ether to interact with the d-f hybrid orbital electron of cesium. Studies show that the d-f hybrid orbital is absent in sodium (Na) and potassium (K) ions and thus, the selectivity of the macrocyclic ligand for cesium is highly optimal. Easy scaling up and low power consumption in nuclear wastewater processing are the main advantages of the d-f hybrid adsorbent and less waste is produced. Research shows that the adsorption of cesium with

OBPX22C6 is better at low pH ranges. Notwithstanding, the high efficiency of the OBPX22C6 in the adsorption of cesium, is affected by co-existing metal ions.²⁹

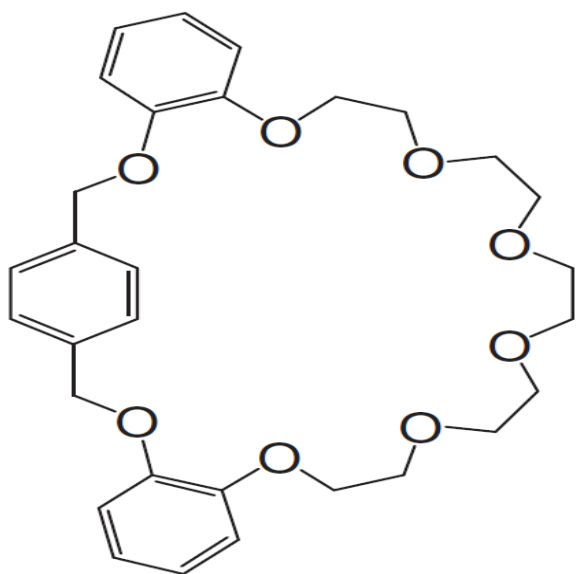


Figure 4: O-benzo-p-xylyl-22-crown-6-ether.²⁹

Similarly, 1,3-[(2,4-diethylheptylethoxy) oxy]-2,4-crown-6-Calix [4] arene (Calix [4] arene-R14) is found to be one of the most promising extractant of cesium among crown ethers. This is as a result of the cavity of its ligand which matches well with the ionic radius of cesium. Calix [4] arenes R14 have higher affinity to remove cesium from wastewater. Group of arenes with similar structures are shown below in Figure 5.³⁰

Ion-exchangers are another kind of adsorbents that have been very useful in removing cesium because of their chemical and radiation stabilities, granulometric properties suitable for column operation and high ion-exchange capacity, and adsorption efficiency.³¹ They demonstrated good selectivity in the processing of wastewater containing cesium and the recovery of valuable metals. Inorganic ion exchangers of the class of tetravalent metal acids have appeared as promising effective materials due to their vital applications in separation science. For example, zirconium-based ion-exchangers have gained interest because of their good selectivity, reproducibility and excellent ion-exchange behavior.

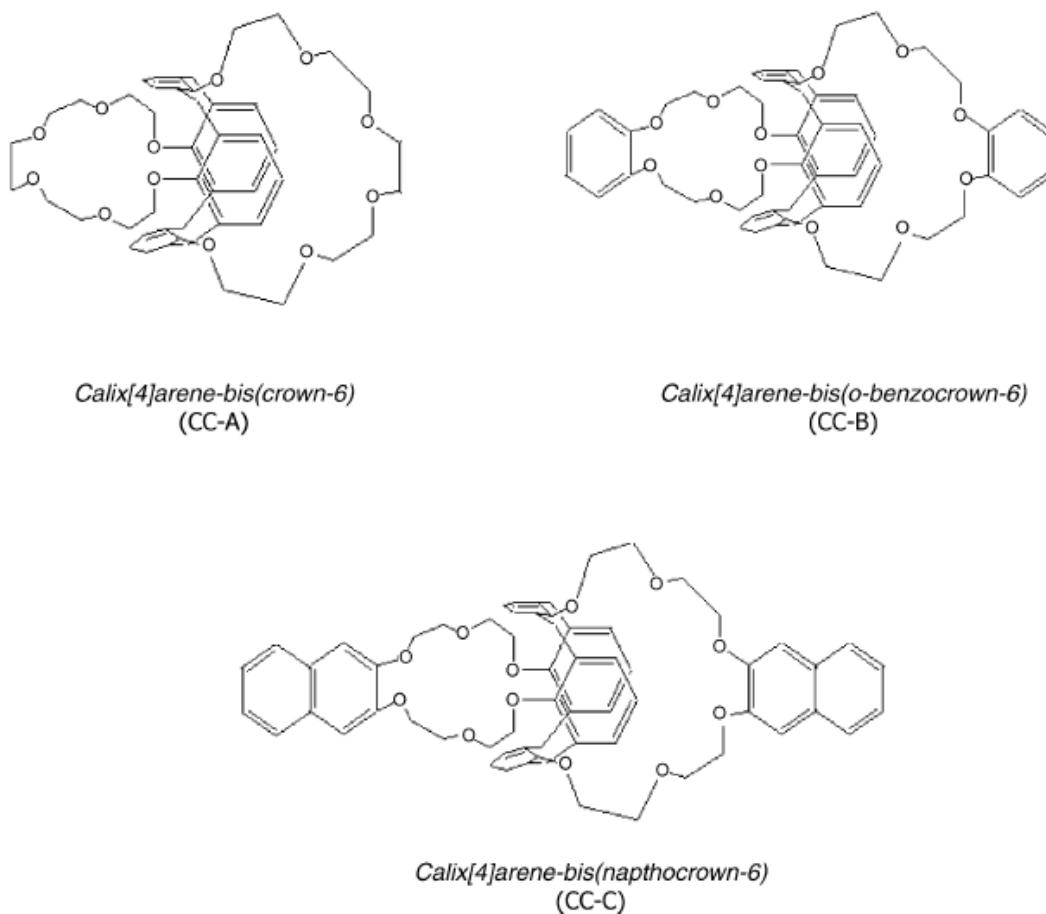


Figure 5: Structures of Calix [4] arenes R14.³⁰

Nevertheless, ion-exchange studies with crystalline materials are often complex because of the formation of new crystalline phases. Amorphous ion exchangers, for example, zirconium (IV) seleniodate, have advantage such as easy preparation. Their granular nature makes them suitable for column operation and they are more preferred than crystalline forms. Besides, they are quite stable in acidic medium.³²

Studies show that adsorption of cesium in clay unceasingly increased to attain a maximum percent at pH of 3. There was a change in the mechanism involved in initial and final stages of adsorption process at higher pH values and adsorption was almost constant throughout this pH values. Since the cesium cation has a large ionic radius and a small hydration number, it can compress the electric double layer around adsorbent particles and reduces the electrokinetic potential that favour its adsorption.³³

Clay colloids are also one of the effective means of adsorption of cesium, significantly enhancing its transport in ground water. Clay colloids exhibit small size and they can remain suspended in groundwater and be transported. Also, their large surface area enhances adsorption capacity for high solubility radionuclides such as cesium. Owing to the very small hydration energy of cesium, it can preferentially interact and adsorb to the surface of clay colloids.³⁴ The coefficient of distribution of cesium and its percentage adsorption increases with pH. This effect may be due to the presence of amphoteric OH groups on the surface of clay colloids that can either be protonated at low pH or deprotonated at a high pH. Thus, at higher pH, the negative charge on the clay increases and the adsorption of cesium ion also increases. Though the clay colloids are effective in adsorption of cesium, their efficiency is drastically reduced in the presence of high concentrations of sodium and calcium ions.³⁵

Insoluble hexacyanoferrates are other substances that have been employed for removing cesium from liquid wastewater containing radionuclides such as cesium. Research shows that insoluble hexacyanoferrates shows high affinity and selectivity for cesium ions. However, this method has certain disadvantage such as pressure drop when used in column application. This can be reduced by attaching supporting material such as polyacrylonitrile (PAN). PAN is an organic binder with good solubility in polar organic solvents, immobilization properties, and strong adhesive forces with inorganic materials. Other studies conducted on PAN-based potassium nickel hexacyanoferrate (II) $K_2Ni(H_2O)[Fe(CN)_6]$ showed high selectivity for removal of cesium from liquid wastewater.³⁶

Furthermore, copper ferrocyanide $Cu_2[Fe(CN)_6]$, CuFC, is an inorganic metal complex that has been used extensively to remove cesium from liquid waste due to its good adsorption property. It also has high affinity for cesium over a wide pH range. However, CuFC adsorption capacity may be reduced by mass or volume occupied by the support

materials and this causes the kinetics of adsorption to be slower due to the mass transfer within the material.³⁷

The application of electrocoagulation process for removing cesium from aqueous solution demonstrated high efficiency for removal of cesium from wastewater. This method uses different anode materials such as aluminium, iron, magnesium, and zinc. With galvanized iron as a cathode, it demonstrated 96 % removal of cesium. Magnesium was used as the cathode and the adsorption process follows the second order kinetics model with good correlation of Langmuir and Freundlich adsorption isotherm model. Langmuir adsorption isotherm favors monolayer coverage of adsorbed molecules for adsorption of cesium.³⁸

Silicate-based multifunctional nanostructured materials with magnetite and Prussian blue showed effective removal of cesium ions from aqueous media by avoiding the use of organic solvents. This method is also effective even at high concentration of sodium chloride which allows their application in the removal of radioactive ¹³⁷Cs. It is easy and has quick recovery of the pollutant -loaded adsorbents by means of a magnet.³⁹

However, these adsorption techniques have some disadvantages associated with their application. There are number of cations such as potassium (K) and sodium (Na) that can block their sorption sites, hence they must be pre-treated with chemicals before use. Also, inorganic adsorbents are expensive and very difficult to separate from solutions because of their microcrystalline nature which causes secondary waste disposal problems.⁴⁰

Heteropolyacids (HPAs)

Heteropolyacids are complex acids containing oxygen, hydrogen, non-metals and metals such as molybdenum, vanadium or tungsten. They form a conjugate anion known as polyoxometalate and they have a well-known structure such as Keggin ($H_nXM_{12}O_{40}$) as shown in Figure 6 and Dawson ($H_nX_2M_{18}O_{62}$).⁴¹ The X in the Keggin structure represents the

central atom while M represents the heteroatom. The heteroatom is either tungsten (W) or molybdenum (Mo) while the central atom is either phosphorus (P) or silicon (Si).⁴²

HPAs' unique catalytic activity is the result of their super acidity.⁴³ The strong acidity of HPAs is caused by delocalization of negative charge on large anions with Keggin structure. HPAs can form insoluble salts with cesium metal cations.⁴⁴

When the heteroatom of HPA is tungsten or molybdenum, it makes it highly active in many catalytic reactions such as condensation, hydration and polymerization.⁴⁵ HPAs demonstrate unique properties such as high thermal stability and high proton mobility which is attributed to their abilities to catalyse several reactions in both heterogenous and homogenous catalysis systems. Phosphotungstic acid (PTA, $H_3PW_{12}O_{40}$) is known to be the strongest HPA with Keggin structure and it is widely used in catalytic hydrolysis and dehydration.⁴² Hence, HPAs have been widely used as acidic, oxidation and electrophilic catalysis in industries. They are environmentally friendly and harmless. Therefore, they are solid acids that can replace harmful solutions such as sulphuric acid (H_2SO_4) and hydrogen fluoride (HF).⁴⁶

Pure HPAs have certain limitations in catalytic applications due to their low surface area and non-porosity. Therefore, for improvement of their catalytic activity, they should be immobilized onto a support with large surface area. Silica, zeolites, mesoporous carbon, and alumina are examples of these supports that have been studied and concluded to be efficient. Increasing the concentration of their acidic sites will also enhance their catalytic activity.⁴⁷

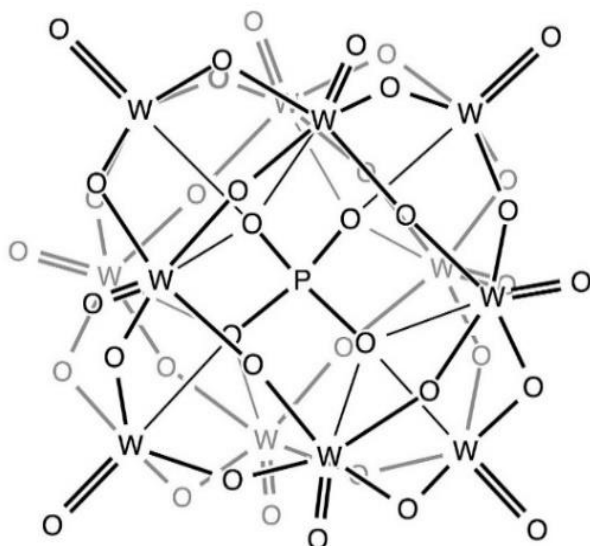


Figure 6: Keggin structures of $H_3PW_{12}O_{40}$ (Walter G. Klemperer)

Immobilization of HPAs

Impregnation Method

Several techniques have been applied in the immobilization of HPAs. Impregnation is one of the common methods for immobilization of HPAs such as PTA on several supports. Studies showed that the catalytic activity and the stability of HPAs depend on the properties of the support, the type of HPA used, and the concentration of the impregnating solution. The impregnation of mesoporous carbon supports with PTA and molybdophosphoric acid ($H_3PMo_{12}O_{40}$) showed that carbon is a suitable support for HPAs. Studies on removal of cesium from liquid waste using impregnated zeolite materials showed higher selectivity and capacity for Cs. Natural and synthetic mordenite also demonstrated high selectivity for Cs. This method was used for low-level radioactive waste with higher improvements in the distribution coefficient of cesium and it is a cheaper method.⁴⁸ However, impregnation method is not effective since physically adsorbed PTA on the support can easily leach out.⁴⁹

Covalent Immobilization

Chemical immobilizers provide one promising means of removal of cesium from aqueous solutions. Generally, immobilized chemicals have high affinity for cesium ions even

at highly acidic conditions. There are a lot of differences in chemical immobilizers in their adsorption capacity for cesium. A study was conducted on immobilization of HPA on mesoporous materials (SBA-15 and MCM-41) by chemical bonding with the introduction of amine groups into the system during aminosilylation procedure. The method resulted in strong anchoring of the heteropolyanions and prevented leaching of HPAs.^{50, 51}

Seaton et al. conducted a research on covalent immobilization of PTA and obtained a hybrid material containing silica gel and PTA. Keggin units of PTA were covalently bonded to silicon (Si) atoms via oxygen bridges. It was observed that covalent Si-O-W bonding demonstrated high stability of PTA against leaching. It was also stable in water and did not decompose in neutral and acidic media. In recent time, researchers have started to focus their attention on this method of immobilization to eliminate the drawbacks of impregnation method.⁵²

Research Objectives

The objective of this work was the synthesis and the instrumental characterization of H-PTA/SiO₂, an adsorbent for removing cesium from the environment. In addition, granulation of H-PTA/SiO₂ with an inorganic binder; aluminium oxide, γ -Al₂O₃, and its effect on the performance of the adsorbent has been characterized as well. Covalent immobilization method will be employed to avoid leaching and the product obtained using this method was expected to be more stable than the product obtained using impregnation method. Finally, an alternative analytical method for determination of surface acidity of base-sensitive materials has been developed.

CHAPTER 2

EXPERIMENTAL/METHODOLOGY

Materials Used

The precursors for the adsorbent (H-PTA/SiO₂, **1**) synthesis, phosphotungstic acid hydrate (PTA) and tetraethyl orthosilicate (TEOS): were purchased from Acros Organics (Morris Plains, NJ). Pluronic P123 with MW=5800, a pore-forming agent, was purchased from Sigma Aldrich (St. Louis, MO).

The salts used in the adsorption studies, cesium chloride (CsCl), potassium chloride (KCl) and sodium chloride (NaCl), were purchased from Fischer Scientific (Pittsburg, PA).

The base used for acidity determination, pyridine was purchased from Acros Organics (Morris Plains, NJ).

The binder used for the adsorbent, aluminium oxide, γ -Al₂O₃ (**2**) was purchased from Strem Chemicals, Incorporated (Newburyport, MA). The solvents used for the adsorption studies were ethanol, tetrahydrofuran (THF) and acetone.

Synthesis and Granulation

Sol-gel Method

The active material for the adsorbent, **1** was synthesised by sol-gel method and the procedure was adapted from an earlier published article.⁵³ Three solutions were prepared: 50 g of Pluronic P123 was dissolved in 150 mL of ethanol, and separately, 18 g of PTA and 72 g of TEOS were dissolved in 50 mL of ethanol. To obtain the highest effectiveness of the adsorbent, the initial contents of the reagents were chosen from data obtained from the previous article. The solutions of TEOS/PTA and 20 % HCl (150 mL) were simultaneously added dropwise to the solution of the surfactant under stirring. The reaction mixture obtained was then refluxed for 24 h. The gel-like mixture obtained was filtered and washed with deionized water to completely remove all the acid in the gel. It was further rinsed with

acetone, air-dried overnight and calcined at 500 °C for 5 h. This temperature was chosen based on literature because it is enough for complete removal of the template.⁵⁴ The Keggin structure was still stable at these conditions.

The preparation of Cs-exchanged material, Cs-PTA/SiO₂ (**3**) was done by mixing 8.2 g of **1** with 100 mL of 0.13 M solution of CsCl. The mixture was stirred overnight, washed by deionized water, and air-dried overnight.

Granulation Process

For obtaining granulated adsorbent, **1** and **2** were mixed and dispersed in deionized water. The mixture was then sonicated in a FS20D ultrasonic bath for 30 min and filtered afterwards. The dry product obtained **1-2** was calcined at 300 °C for 3 h. It was then compressed into tablets at a pressure of 7 metric tons and separated (1-2 mm fraction) using Fisher Scientific test sieves.

Using this procedure, three samples (2 g) each were prepared by mixing **1** and **2** with different ratios. First sample was prepared with the 1:1 ratio, second sample with the 1:9 ratio and third sample with the 3:7 ratio. Composition of the dry products were: **1-2** (10 %), **1-2** (30 %), and **1-2** (50 %).

Structural and Instrumental Characterization

X-ray Fluorescence (XRF) Study

X-Supreme 8000 XRF analyser (Oxford Instruments, Abingdon, UK) was used to determine the elemental compositions of the material.

Elemental Analysis

The concentration of cesium (Cs) and tungsten (W) in the samples were determined by atomic absorption spectrometry (AAS) using Shimadzu AA-6300 Spectrometer (Kioto, Japan). Samples for measurement were prepared by dissolving the materials in 48 % HF (VWR International, Radnor, PA). This was then followed by neutralization by

NH₄OH (25 %) to pH=7. 0.1 g of adsorbent was dissolved in 10 mL of HF and diluted after neutralization to approximately 25-30 mL. This would result in a concentration of tungsten (W) in the solution in the range of 100-500 ppm. This was the calibration curve chosen for analysis of W, which is very high for a typical element in AAS, but it worked using the high temperature burner. For calibration of Cs, solutions in the range 5-50 ppm were prepared.

Fourier-Transform Infrared (FT-IR) Spectroscopy

All FT-IR spectra were recorded in KBr pellets on Genesis II spectrometer (Shimadzu, Kyoto, Japan).

Nuclear Magnetic Resonance (NMR) Spectroscopy

Solid state NMR spectra were acquired on a Bruker AVANCE 400 spectrometer (Rheinstetten, Germany). For ³¹P spectra recordings, 85 % H₃PO₄ was used as the reference standard based on the literature. It was conducted at 162 MHz, pulse length: 5 μs, delay time: 10 s, number of scans: 10,000.

²⁷Al spectra were recorded at 104.26 MHz, pulse length: 3 μs, delay time: 1 s, number of scans: 128. Samples were dried at room temperature in vacuum until constant weight was obtained before taking all measurements.

Surface Acidity

Reversed titration method was used to measure the concentrations of surface acidic sites in the samples. 0.1 g of the sample was dehydrated at 100 °C overnight and dispersed in 6 mL of 0.012 M solution of pyridine in THF. The solvent was dried using NaOH before titration. The solvent (THF) was chosen because Keggin units are unstable in aqueous media at high pH. It was filtered, diluted with 100 mL of deionized water, and the amount of pyridine remaining was determined by titrating with 0.02 M HCl using Orion 350 pH meter (Thermo Scientific, Pittsburg, PA) until pH=3. Figure 7 below shows an outline of the reaction of HPA with pyridine.

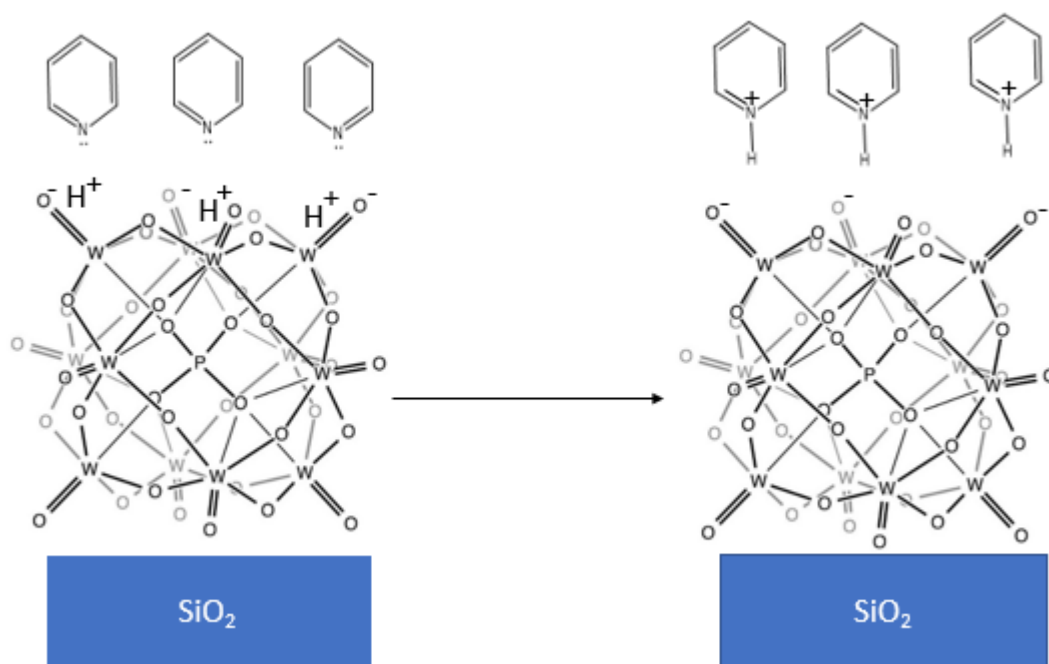


Figure 7: An outline of the reaction of HPA with pyridine

Scanning Electron Microscopy (SEM) and Transmission Electron Microscopy (TEM)

SEM images were obtained on a Zeiss DSM 940 scanning electron microscope (Oberkochen, Germany) at 20 kV. Before imaging, the samples were coated with gold.

TEM images were obtained on a JEOL 1230 electron microscope (Tokyo, Japan) at 80 kV. Prior to measurement, the samples were dispersed in a 50 % ethanol solution using a W-385 sonicator (Heat Systems Ultrasonic, Newtown, CT) for 2 min before imaging.

Particle Size Distribution

Particle size analysis was done using dynamic light scattering method on a Zetasizer Nano ZS90 (Malvern, UK). Prior to measurement, samples were sonicated for 5 min.

X-ray Diffraction (XRD)

XRD patterns were recorded on a Dron 2.0 diffractometer (St. Petersburg, Russia) using an X-ray tube with a copper anode and a nickel filter at 30 kV and 15 mA. The patterns were collected in the range of angles 2θ from 5 to 40° .

Porosity

The porous characteristics of the samples were determined using Quantachrome Nova

2200e porosimeter. (Boynton Beach, FL). The samples were degassed at 300 °C in a vacuum for 2 h before measurement. N₂ was used as an adsorbate for recording the adsorption/desorption isotherms. The Brunauer–Emmett–Teller (BET) surface areas were calculated from the adsorption branch of isotherms to be in the range of P/P₀ = 0.2-0.4.

Total pore volumes, pore size distributions, and average pore diameters were determined using Density Functional Theory (DFT) method. Saito–Foley (SF) method was used to calculate the micropore volumes and average diameters. NovaWin v.11.02 software was used to perform all calculations.⁵⁵

Thermogravimetric Analysis (TGA) and Differential Scanning Calorimetry (DSC)

TGA was provided by Robertson Microlit Lab. (Ledgewood, NJ). TGA was conducted on a Perkin Elmer TGA 7 analyser.

DSC analysis was also provided by Robertson Microlit Lab. (Ledgewood, NJ). DSC analysis was conducted on a Pyris Diamond differential scanning calorimeter (Perkin Elmer, Waltham, MS) in a sealed pan. The heating rate was 10 °C/min.

Adsorption Studies

Batch Tests

Batch tests were conducted by dispersing 2 g of the adsorbent in 10 mL of CsCl solution with Cs⁺ contents 0.15, 0.37, 0.75, and 1.5 mmol/L. The mixture was incubated for 2 hours at 40 °C in a circulating water bath, (Thermo Scientific, Pittsburg, PA). The remaining concentration of Cs in the solutions were then measured using AAS.

Column Tests

Column tests were conducted on **1-2** (50 %) from CsCl solutions using 0.15 mmol/L concentration. Also, mixed solutions contained 0.15, 0.37, 0.75, and 1.5 mmol/L of KCl or NaCl. The solutions were then passed through a column containing 2 g of the granulated

adsorbent (1.8 cm^3) with the flow rate of 0.08 mL/min ($0.044 \text{ mL/cm}^3_{\text{ads.}}\text{min}$). The samples (2 mL) were collected every 25 min and analysed by AAS.

CHAPTER 3

RESULTS AND DISCUSSION

Synthesis and Granulation

Sol-gel Synthesis and Ion-exchange

A gel-like mixture was formed about 40 min after the start of reflux. Organic components were completely removed within the temperature range of 480-500 °C. Product **1** yielded 21 g, corresponding to a complete conversion of TEOS and PTA to the product.

Sample **3** was found to contain 17.1 % of PTA (0.059 mmol/g) and 2 % of Cs (0.15 mmol/g). Hence, the molar ratio of **3** after adsorption was 2.55. Characteristics of **1**, **2**, **3**, and other synthesized materials are shown in Table 1 below.

Granulation

After granulation process, three products were obtained. Their compositions were: 90 % of **1** and 10 % of **2** [**1-2** (10 %)], 70 % of **1** and 30 % of **2** [**1-2** (30 %)], and 50 % each of **1** and **2** [**1-2** (50 %)].

Structural and Instrumental Characterization

XRF Study

Based on X-ray fluorescence study, the elemental composition of **1-2** (50 %) was: Al₂O₃, 43.77 %; SiO₂, 51.59 %; WO₃, 4.32 %; P₂O₅, 0.32 %. Hence the material contained 4.73 % of PTA.

FT-IR Spectroscopy

Figure 8 below shows the FT-IR spectrum of **1** with characteristic bands of silica gel at 803 cm⁻¹ (ν_sSi–O–Si), 1080 cm⁻¹ (ν_{as}Si–O–Si), 1638 cm⁻¹ (adsorbed water), and 3480 cm⁻¹ (νOH). The band at 958 cm⁻¹ (ν_{as}W–O–W) demonstrated the presence of Keggin units in the silica structure.⁵⁴ The following typical bands were observed in the spectrum of **2**: a broad band at 835 cm⁻¹ is ascribed to the tetrahedrally-coordinated Al³⁺, multiple bands at

1627-1654 cm^{-1} of adsorbed water, and the band at 3448 cm^{-1} (νOH). In **1-2** (50 %), the band at 835 cm^{-1} was shifted to 817 cm^{-1} in respect to **2** whereas in the **1-2** (10 %), and **1-2** (30 %) it was not detected.

Table 1: Characteristics of H-PTA/SiO₂, Cs-PTA/SiO₂, H-PTA/SiO₂ bound with $\gamma\text{-Al}_2\text{O}_3$.⁵⁴

Properties	Samples					
	1	2	1-2 (10 %)	1-2 (30 %)	1-2 (50 %)	3
BET surface (m^2/g)	286.9	230.7	414.7	424.1	574.1	294.1
Pore volume (cm^3/g)	0.38	0.64	0.32	0.39	0.65	0.27
Average pore half width (\AA)	16.6	7.1	3.3	3.3	3.3	9.2
Micropore volume (cm^3/g)	0.073	0.06	0.10	0.11	0.15	0.073
Average micropore size (\AA)	2.26	0.45	0.45	0.45	0.45	2.26
Particle size (nm)	1163	736	744	754	656	642.9
PDI	0.165	0.16	0.80	0.66	0.47	0.286
Acidity (mmol/g)	0.32	0.37	0.44	0.35	0.21	0.47

NMR Spectroscopy

Solid state ^{31}P NMR spectrum of **1-2**(50%) is presented in Figure 9 below. Two peaks were observed: an intense peak at -14.7 ppm and a shoulder at -5.5 ppm. The first peak is characteristic for Keggin units of bulk hydrated phosphotungstic acid. The shoulder signifies phosphorus species from fragmented Keggin units.⁵⁶

Solid state ^{27}Al NMR spectrum of **1-2**(50%) is shown in Figure 9 below. Two major peaks were shown at 14.4 ppm and 61.5 ppm and were characteristic of $\gamma\text{-Al}_2\text{O}_3$. They correspond to hexa-coordinated (AlO_6) and tetra-coordinated (AlO_4) aluminium species, respectively. Also, a small sharp peak at 4.7 ppm was found in commercial $\gamma\text{-Al}_2\text{O}_3$. It is distinctive for hydrated aluminium cations $\text{Al}(\text{OH})_n(\text{H}_2\text{O})_{6-n}^{(3-n)+}$ ($n = 0-2$).⁵⁷

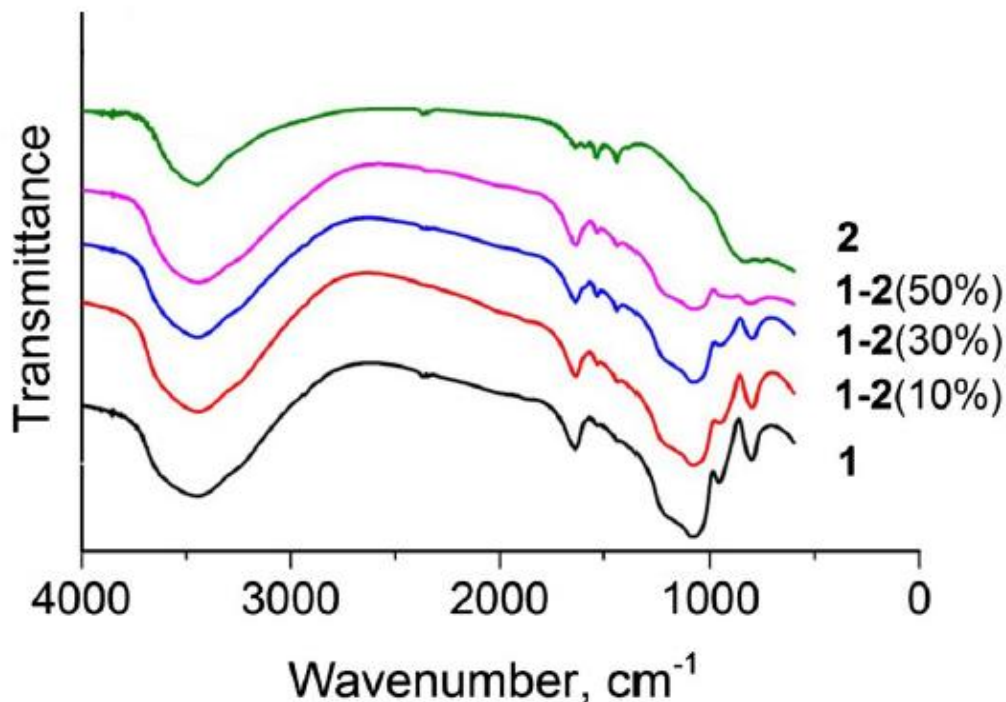


Figure 8: FT-IR spectra of **1**, **2**, **1-2** (10 %), **1-2** (30 %) and **1-2** (50 %).⁵⁴

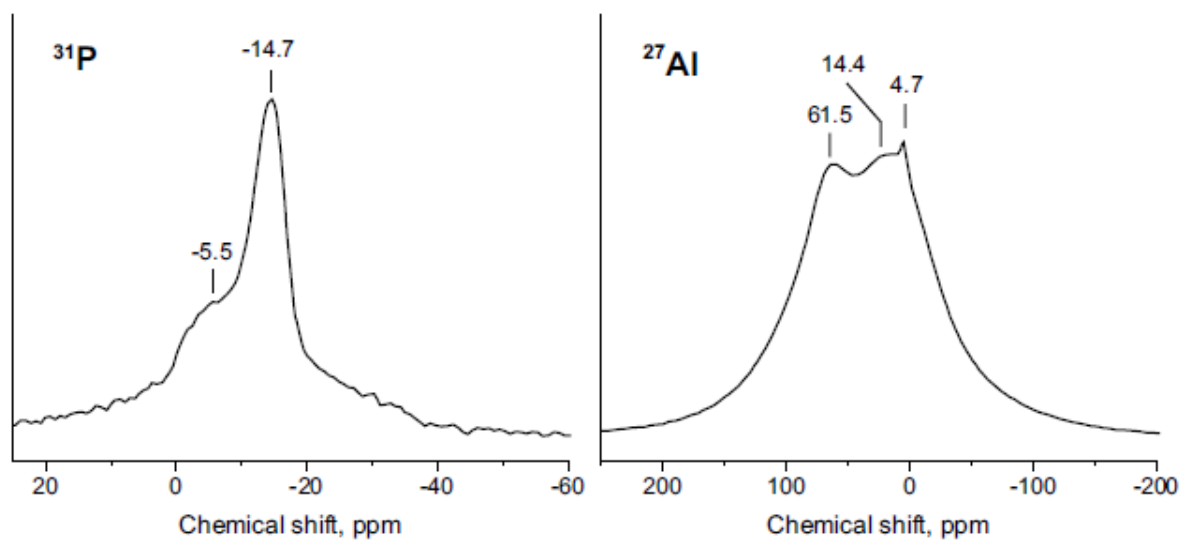


Figure 9: ³¹P and ²⁷Al NMR spectra of **1-2** (50 %).⁵⁵

Surface Acidity

The results obtained from the determination of surface acidity showed the presence of highly acidic sites. After adsorption of Cs, the number of acidic sites increased as shown above in Table 1.

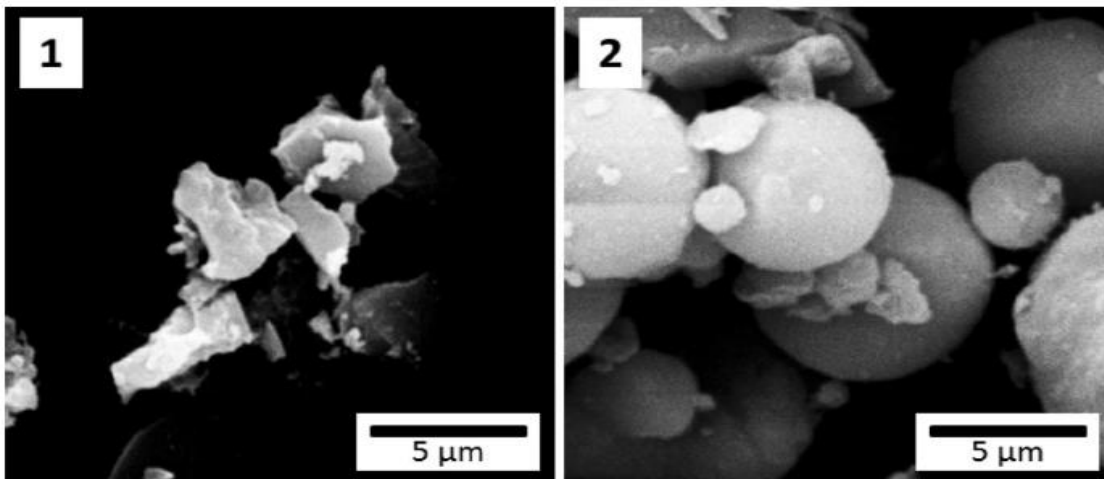
SEM and TEM

Sample **1-2** (50 %) consisted of two solid phases as shown below in Figure 10.

It also consisted of spherical particles of the aluminium oxide having diameters 1-5 μm which were covered by smaller particles of silica having irregular shapes and their sizes vary from 0.1 to 1 μm . It was found that particles tend to agglomerate. However, large conglomerates of silica particles were absent.

TEM imaging showed microstructure of the silica particles with irregular shapes. They were formed by small spherical nanoparticles of 5-20 nm diameters as shown below in Figure 10. Dark spots were seen in some of the particles which indicate the presence of tungsten.

(a)



(b)

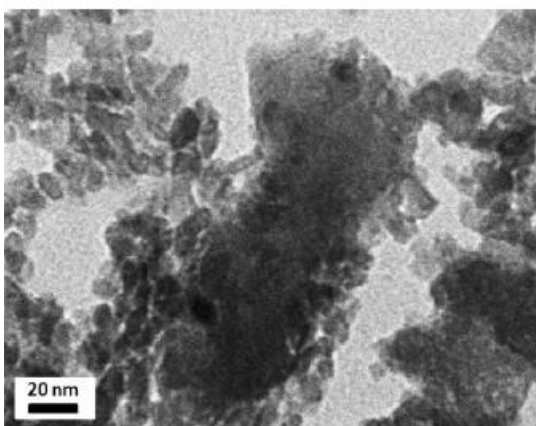


Figure 10: (a) SEM images of **1**, and **1-2** (50 %) ⁵⁴, and (b) TEM images of **1-2** (50%) ⁵.

Particle Size Distribution

Figure 11a shows the particle size distribution of H-PTA/SiO₂, γ -Al₂O₃ and **1-2** (50 %). Three groups of particles were observed in sample **1**. Larger particle sizes were found within 300-2000 nm which represent 66 %, and the smaller particles between 100-300 nm indicates 31.7 % of the material. The remaining 2.2 % consisted of conglomerates up to 6000 nm. The binder (**2**), consisted of particles within the range of 700-1100 nm. Curve **1-2** (50 %) represents the bound material. Large conglomerates of silica particles were almost absent in the bound material. Figure 11b shows particle size distribution of **1-2** (50 %) before (black) and after (red) adsorption of cesium. Before adsorption of cesium, particles sizes were found in the range of 900-1800 nm. The particle size distribution changed after adsorption of Cs⁺ and this triggered a significant decrease of the average size as shown above in Table 1. It was found within the range of 400-1000 nm. The polydispersity index (PDI) of the material decreased after adsorption due to deagglomeration. Also, the particle size distribution of γ -Al₂O₃ and its effect in all bound materials are shown in Table 1 above.

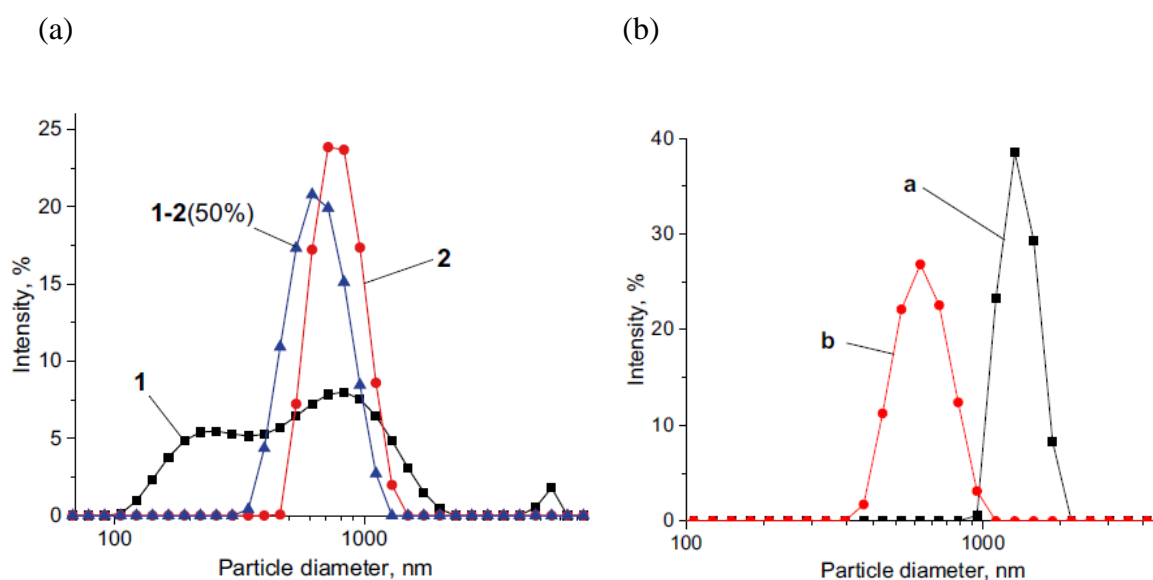


Figure 11: (a) Particle size distribution of **1**, **2**, and **1-2** (50 %).⁵⁴, (b) Particle size distribution of **1-2** (50 %) before (black) and after (red) adsorption of cesium.⁵⁵

XRD Study

XRD patterns showed presence of amorphous silica gel as shown in Figure 12 below. The diffractogram shows a broad peak at 26.2° . Bragg's equation was used to determine the d-spacing (average size of repeating units) which corresponds to this peak that was found at 0.34 nm. The characteristic patterns of $\gamma\text{-Al}_2\text{O}_3$ were found to be weak and their positions at $2\theta = 20.4^\circ, 33.0^\circ, 37.2^\circ$ and 39.2° correspond to (111), (220), (311) and (222) planes, respectively.⁵⁸ Also, PTA patterns were not identified because of its low content but peaks at $2\theta = 10.2^\circ$ and 21.2° might be pertaining to its (110) and (222) planes.⁵⁹

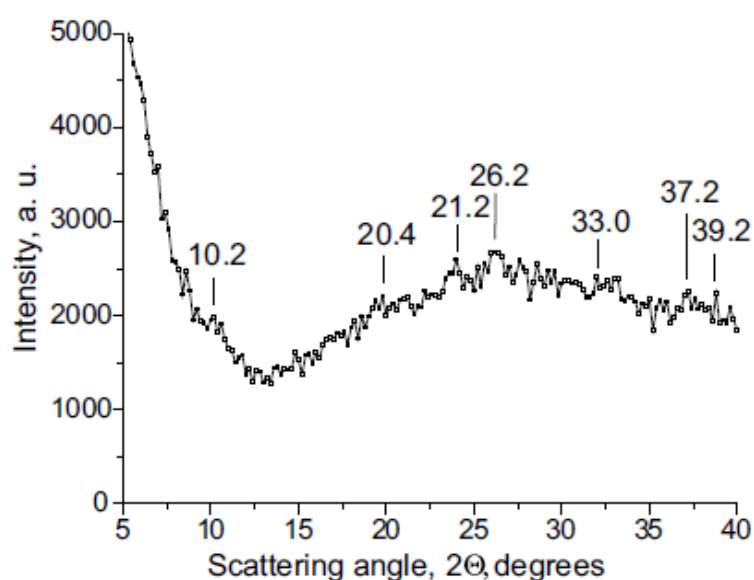


Figure 12: XRD patterns of 1-2 (50 %).⁵⁵

Porosity

Non-bound material **1** demonstrated a mesoporous structure but contained a significant fraction of micropores in its structure with macropores being absent. The pores were classified into five distinctive groups by size: 1.5 and 1.8 nm (micropores), and 2.8, 3.3, and 4.2 nm (mesopores). The micropore and total pore volumes decreased after adsorption of Cs^+ likewise the BET surface area as shown above in Table 1. N_2 adsorption/desorption isotherms in Figure 13 belong to the type IV. The binder, $\gamma\text{-Al}_2\text{O}_3$, was mesoporous, however, its pore size distribution showed a high volume of macropores. The various sizes of the pores

are 4.5-6.2 and above 6.3 nm. The loop at $P/P_0=0.7-1.0$ signifies an important contribution of mesopores formed by inter-crystalline spaces in $\gamma\text{-Al}_2\text{O}_3$. The hysteresis loop obtained can be classified under H1 type, and this is typical for well-defined cylindrical mesopores.

Isotherms of N_2 adsorption/desorption and pore size distributions of raw and bound materials are shown in Figure 13c and 14 (a, b). The shape of hysteresis loop is characteristic

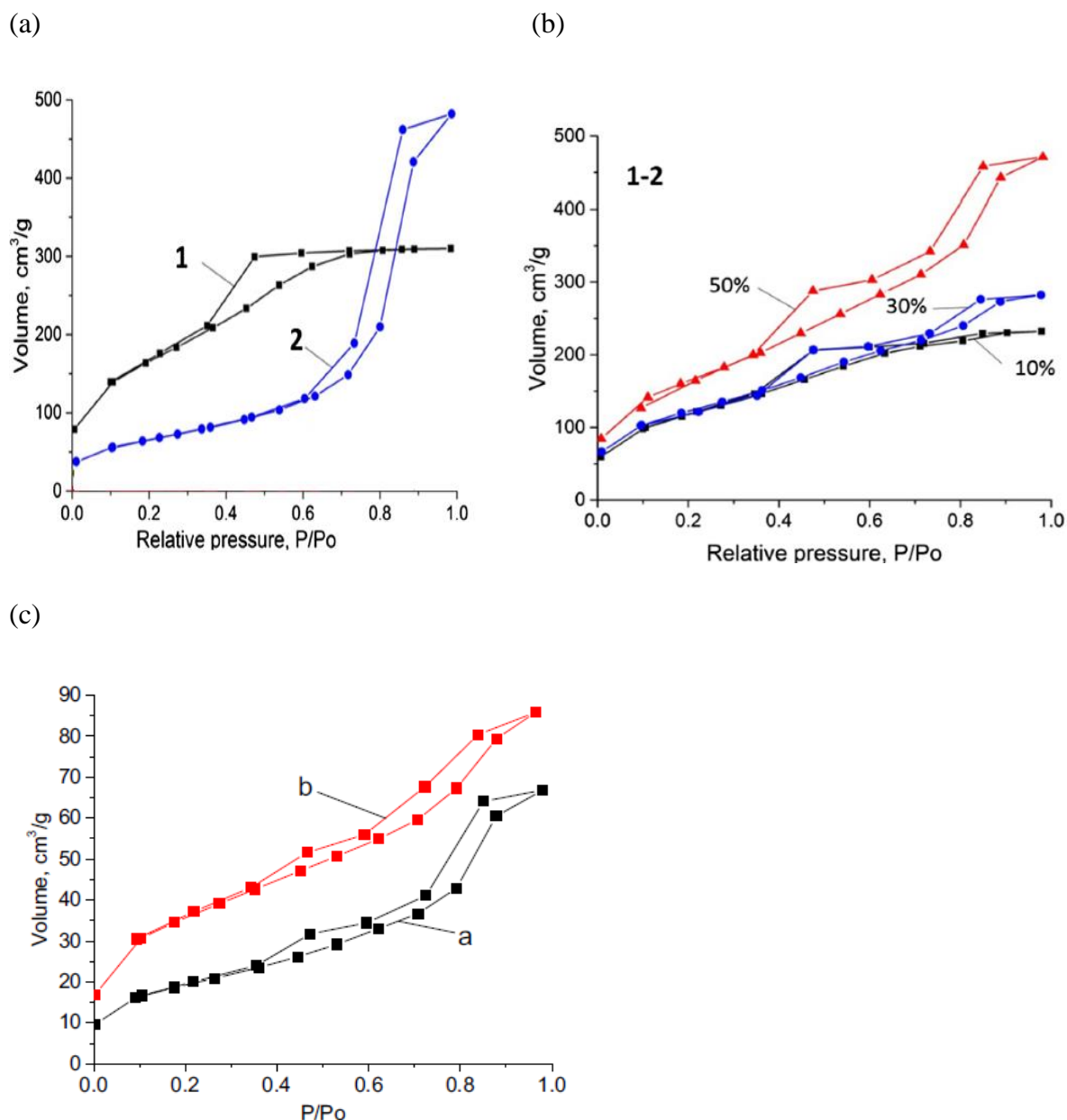


Figure 13: (a) N_2 adsorption isotherm of 1, and 2 (b) N_2 adsorption isotherm of 1-2 (10%), 1-2 (30 %), and 1-2 (50 %) ⁵⁴ (c) N_2 adsorption/desorption isotherms of 1-2 (50 %) before (a) and after (b) adsorption of cesium. ⁵⁵

for bimodal mesostructures which indicates two mesoporous phases. The pores of SiO₂ denote the first step of capillary condensation at the P/Po range of 0.4-0.7 whereas larger pores of γ -Al₂O₃ represent the second step at 0.7-1.0. Figure 14c below shows pore size distribution graph with three independent pore groups. The groups of 5-10 and 12-20 Å represent pores of SiO₂ whereas pores > 20 Å pertain to γ -Al₂O₃. The two maxima at 25 and 35 Å were observed for the last group. Following the adsorption of Cs⁺, a rearrangement of silica pores occurred and the smaller pores with maximum at 7-8 Å increased at the cost of the larger 16 Å pores.

Thermal Analysis

The TGA curve of **1-2** (50 %) showed loss of 4.2 % of its weight in the course of heating up to 100 °C, this can be attributed to evaporation of physically adsorbed water as shown in Figure 15 below. Afterwards, the weight loss (3 %) became gradual up to 480 °C, which can be ascribed to the removal of chemically bonded water in silica gel and alumina. Also, the dehydration of PTA hexahydrate to its anhydrous state occurred at the same temperature. Decomposition of the material became more intensive at 480 and 700 °C and the sample lost 1.3 % of weight. DSC analysis was used to detect the phase change in **1**. The DSC thermogram showed small endothermic peak with the enthalpy $\Delta H = 33.7$ J/g at 164 °C. In addition, an endothermic step was observed between 165 and 214 °C. This can be attributed to the peak at 187 °C in the DCS curve of **1** and it corresponds to a decrease in the PTA lattice size.⁶⁰ The slope of the baseline is due to the gradual change of the specific heat capacity of the sample due to the gradual dehydration that occurred. The change in slope at 540 °C denotes an irreversible decomposition of PTA into P₂O₅ and WO₃.

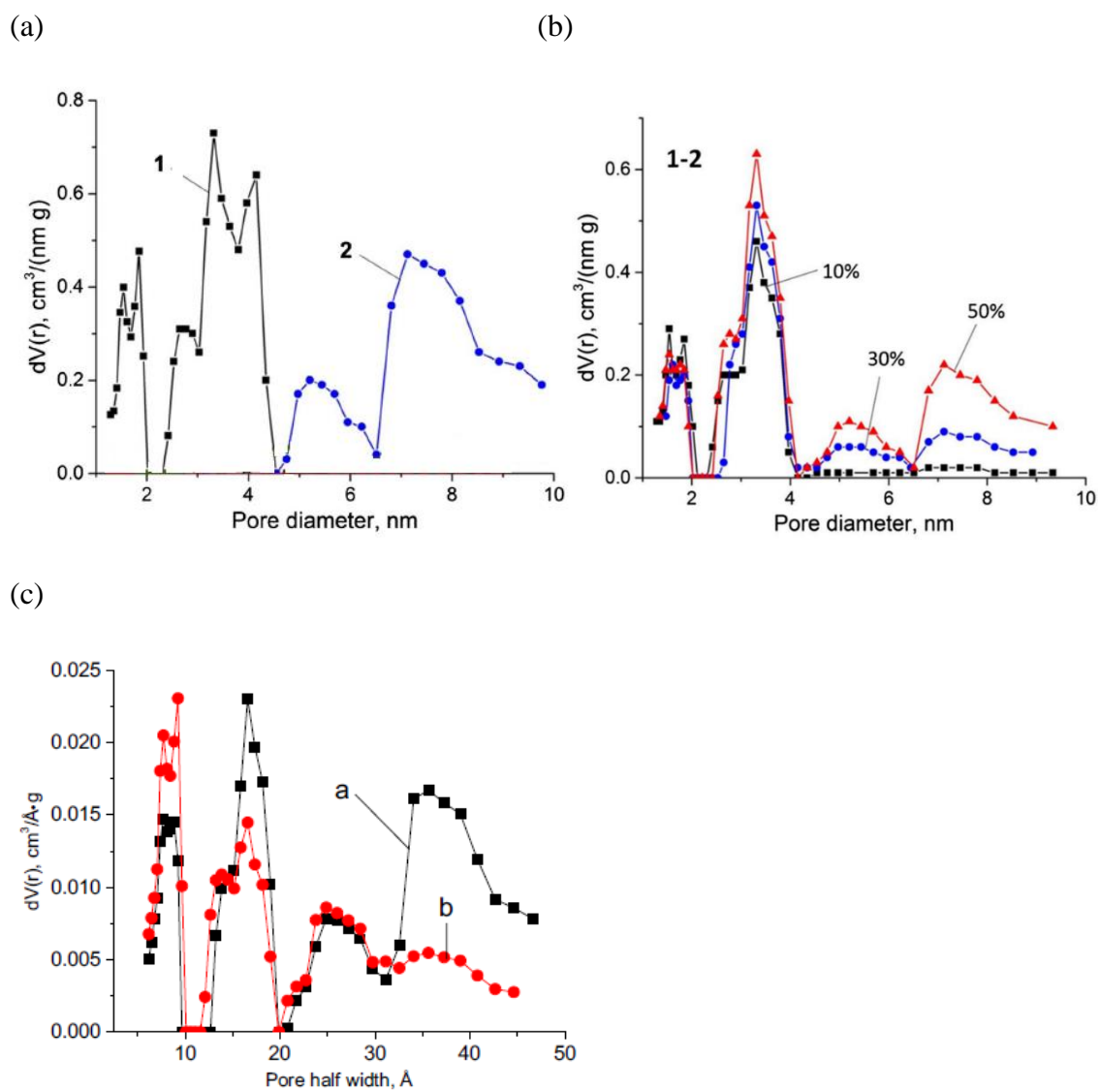


Figure 14: Pore size distribution of adsorbents and bound materials (a) Pore diameter of **1**, **2**⁵⁴ (b) Pore diameter of bound materials (c) Pore half width of before (a) and after (b) adsorption of Cs.⁵⁵

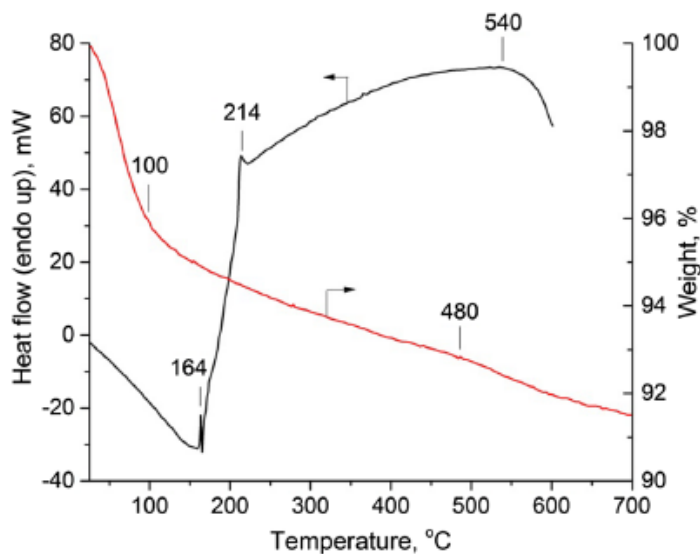


Figure 15: DSC and TGA curves of **1-2** (50 %).⁵⁴

Adsorption Studies

Batch Tests

Based on the study of adsorption of cesium on pure materials, there was high adsorption capacity of pure **1** and very slight ability of the binder to adsorb cesium as shown in Figure 16 below. It was observed that the adsorption capacities of all bound materials were lower as compared to the non-binding material, **1** and the adsorption of cesium decreased with decreasing contents of **1**. This inconsistency can be ascribed to a partial silica pore blocking by a binder. Hence, additional increase of its amount does not make any significant change in the adsorption capacity. Moreover, the adsorption was dependent on the concentration of Cs^+ in the solutions.

Column Tests

The results obtained from column tests showed that the adsorbent demonstrated good adsorption capacity towards cesium as shown below in Figure 17. After adsorption, concentration of Cs^+ cations decreased from 0.150 to 0.029-0.046 mmol/L. Hence, the average concentration of cesium after the experiment was 0.037 mmol/L. There was no effect on Cs^+ adsorption upon addition of NaCl or KCl to the CsCl solution. In all experiments, Cs^+

concentration after adsorption varied between 0.025 and 0.044 mmol/L in the presence of NaCl, and between 0.027 and 0.051 mmol/L in the presence of KCl. However, the values obtained from the experiment varied slightly and this is attributed to non-uniform flow of the solutions through granulated material.

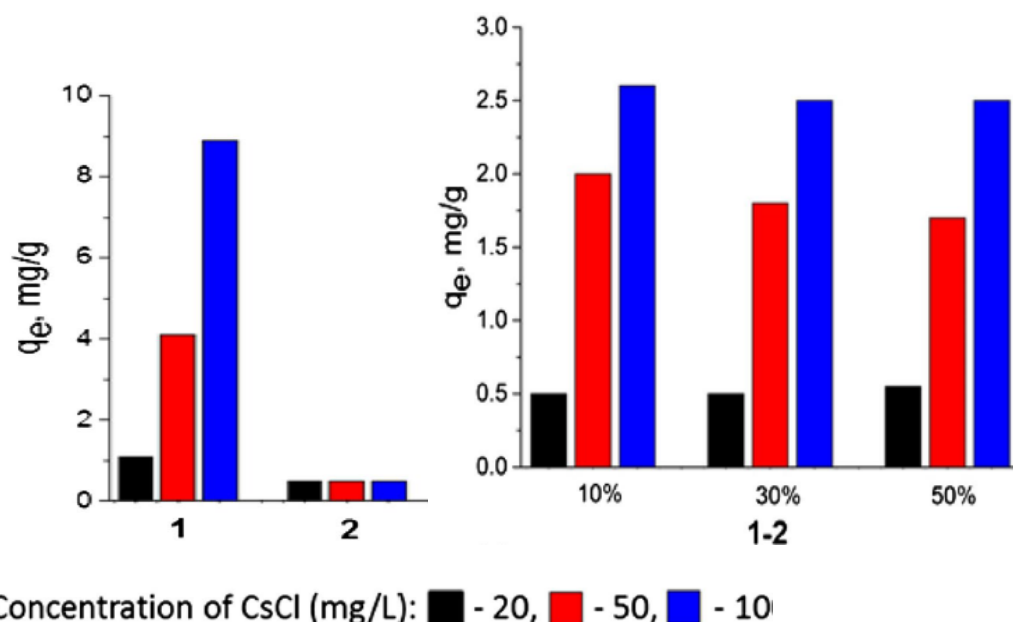


Figure 16: Adsorption of Cs from CsCl solutions (20, 50, and 100 mg/L) on bound materials.⁵⁵

Direct and indirect analysis were used to determine the total amount of cesium adsorbed from 20 mL of the CsCl solution. Also, the dissolution of the Cs-treated adsorbent in HF followed by AAS analysis showed that the content of Cs in the sample was 0.134 mg/g (0.0134 wt %). Therefore, the total amount of adsorbed cesium was 0.268 mg. AAS analysis of CsCl solution after adsorption showed a decrease in concentration by 0.114 mmol/L and this value corresponded to 0.303 mg of the adsorbed Cs (0.0152 wt %), which correlates with the data obtained by direct analysis. The adsorbent maintained a stable adsorption rate and did not show any tendency to decreasing its adsorption ability to the end of the experiment.

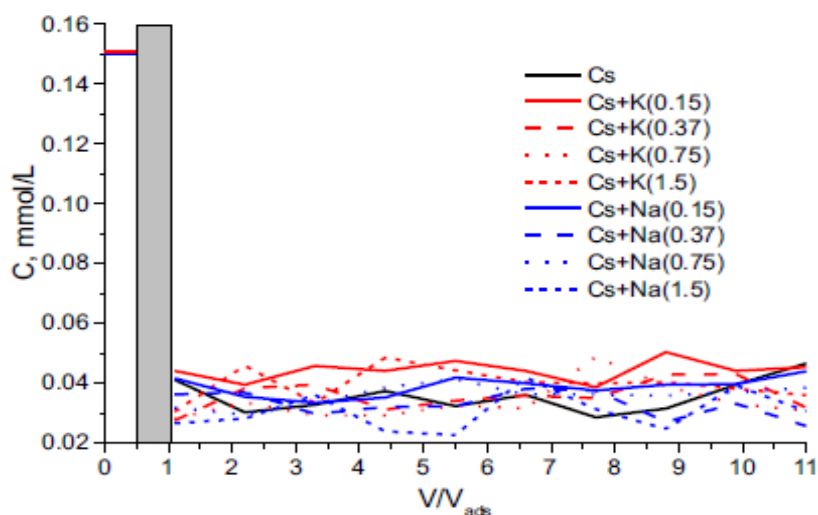


Figure 17: Graph of adsorption of cesium on 1-2 (50 %) from CsCl solution (0.15 mmol/L) and its mixtures with NaCl and KCl (0.15-1.5 mmol/L).⁵⁴

Discussion

As it is clear from the chemistry of adsorption of cesium, adsorption capacity corresponds to the number of adsorption sites, which are embedded Keggin units. Acidic protons of PTA are exchanged by cesium cations. Thus, the adsorption capacity depends on the concentration of accessible acidic protons in the material.

Quantitative determination of surface acidity of porous materials is an important analytical problem in characterization of the adsorbents. Common solid-state titration method is not applicable to the PTA-containing materials. PTA can exist in acidic media only and hydrolyses in basic media to PO_4^{3-} and WO_4^{2-} .⁶⁶ As a result, it decomposes during titration process that made direct titration impossible.

Comparison of the granulated form of an adsorbent with its powder form showed that the former had significant advantages over the latter which had higher permeability, larger bulk density, and easy handling. Therefore, an adsorbent material should be compressible and compactible. The synthesized modified silica gel could not be efficiently granulated in its pure state hence it required a binder. Contrary to silica gel, $\gamma\text{-Al}_2\text{O}_3$ is simply compressible.

Its granules showed excellent mechanical properties concerning elastic and elastic–plastic material behavior.⁶¹ H-PTA/SiO₂ was the active ingredient used and the binder was γ -Al₂O₃.

The Keggin structure of PTA in the adsorbent was not affected when compressed with a binder. The solid state ³¹P NMR spectrum demonstrated similarities to the spectrum of non-bound material.⁵² Two major signals were observed at 14.4 and 61.5 ppm in ²⁷Al spectrum present in the commercial alumina. Nevertheless, a small sharp signal at 4.7 ppm was detected in the spectrum of the raw material.⁵⁸ The reaction between superacidic PTA and γ -Al₂O₃ during the adsorbent processing generated this signal.⁶²

This study showed that the acidity of the materials was dependent on various factors such as contents and accessibility of acidic sites in the porous structure but not limited to this. However, based on the XRF data obtained, their number in bound H-PTA/SiO₂ did not concur related to the contents of PTA, which was 0.016 mmol/g. The titration data and the BET surface area were used to calculate the surface densities of Keggin units and accessible acidic sites in the adsorbent as 0.034 and 0.67 sites/nm² respectively. Also, the formation of additional acidic sites can be attributed to the hydration of Keggin units and the formation of additional surface hydronium cations. Okuhara et al. discussed that the bulk PTA can adsorb up to 17.7 amine molecules per Keggin unit.⁶³

Banerjee et al. showed that aluminum can substitute up to 2.31 protons of PTA with retention of the Keggin unit's structure.⁶⁴ Conversion of these cations from the alumina network to silica-embedded PTA generates additional micropores and increases the number of accessible surface acidic sites. The changes observed in microstructure might be due to the interactions between highly acidic protons of Keggin units and γ -Al₂O₃, consequential to partial neutralization of PTA by Al³⁺ cations.⁶⁵ Table 1 above shows that the acidity of **1-2** (10 %) was even higher than the acidity of any of its components.

TEM image shown above in Figure 10b affirmed nanostructures of these small particles that were formed by nanocrystallites in the range of 10-20 nm. The empty spaces between the nanocrystallites have a width of 2-4 nm, which is attributed to the second group of pores in the pore size distribution graph as shown above in Figure 14c.

The results obtained from particle size distribution study showed that the adsorbent material demonstrated a strong tendency towards agglomeration. The non-bound H-PTA/SiO₂ typically exists in the form of 100-500 nm sized particles.⁵² However, particles of this size ranges were not observed in the bound material, which formed large conglomerates > 1 μm in size as shown in Figure 11a above. The material consisted of two clearly distinct phases as shown above in Figure 10a. Also, smaller particles of H-PTA/SiO₂ were strongly bound to the alumina surface as seen clearly from particle size distribution graph. Unpredictably, the particle size distributions in **1-2** (50 %) was identical to that of the binder but was distinguishable from the pure adsorbent **1**. One of the most prominent characteristics of the bound materials was full absence of particles below 300 nm, even though the fraction in the bound adsorbent was expected to be at least 10-15 %. The mesopore volume and surface area were affected because some part of **1** was embedded in macropores of the binder.

The porous characteristics of the bound adsorbent integrated characteristics of its two components: medium surface alumina binder with larger mesopores, and high-surface H-PTA/SiO₂ with micropores and smaller mesopores.⁵⁴ The porous structure of H-PTA/SiO₂ and the non-modified silica gel were similar, but PTA increased the average pore size and the total pore volume.⁵³

After comparison of the thermal behavior, of **1-2** (50 %) with the data obtained for pure **1**, it is clearly seen that the water content in the bound material was significantly

lower.⁵² Sample **1** lost 16 % of its weight between 25 and 700 °C, whereas the total weight loss of **1-2** (50 %) was just 8.5 %.

At the temperature of the experiment, adsorption of cesium occurs only on embedded PTA sites. Adsorption sites of embedded PTA were characterized, and it was found that they fall into two groups by their accessibilities. The first group have easily accessible sites located on the external surface of crystallites. There are no diffusion limitations, hence adsorption on these sites is fast. The second group have adsorption sites located inside the pores. The rate of intraparticle diffusion limits access to these sites. The adsorption on these sites was slow and the equilibrium establishes after about 1 h. in consideration of the low concentration of Cs⁺ in the solutions, the second group (silanol) provided relatively low contribution to the total adsorption.⁵² The effect of competing cations Na⁺ and K⁺ was negligible in this range of concentrations. The binder also possesses surface functional groups able to adsorb Cs⁺: Al–OH (**2**), however, it did not bind cations of alkali metals irreversibly

Based on the results of column tests, 69-81 % of the initial amount of Cs⁺ was adsorbed at the studied adsorption conditions. For solutions containing K⁺, this value was almost the same: 66-81 %. However, in the presence of Na⁺, it was slightly higher at 70-85 %. The amount of PTA in the adsorbent was 0.016 mmol/g. Considering that each molecule of PTA has 3 exchangeable protons, a maximum adsorption capacity of the adsorbent is anticipated to be 0.048 mmol/g or 0.644 wt % of cesium. However, only 2.08 % of acidic protons in PTA were exchanged by cesium after 250 mins of adsorption.

Specific adsorption per mass of active ingredient of adsorbent was H-PTA/SiO₂ because amount of H-PTA/SiO₂ is lower than the other compositions but adsorption is the same. Adsorption per unit mass of H-PTA/SiO₂ is higher.

Conclusion

To obtain an effective adsorbent for removal of cesium, silica gel containing embedded phosphotungstic acid was granulated with an inorganic binder: $\gamma\text{-Al}_2\text{O}_3$ due to low cost. The obtained material demonstrated high porosity with high BET surface area and contained both micropores and mesopores in its structure. Quantitative determination of surface acidity of porous materials is an important analytical problem in characterization of the adsorbents. This problem was solved by reversed titration after saturation of the materials by anhydrous solution of pyridine. This approach can be applied to analysis of base-sensitive materials of various compositions. The bound material showed effective adsorption of Cs^+ in the presence of cations of other alkali metals. The adsorbent characteristics were changed by ion exchange of H^+ with Cs^+ . Deagglomeration of large particles, and microporosity were observed.

REFERENCES

1. Avery, S. V. Fate of cesium in the environment; distribution between the abiotic and biotic components of aquatic and terrestrial ecosystems. *J. Environ. Radioact.* **1996**, *30*, 139-171.
2. Katoh, T.; Nakamura, S.; Harada, H. Measurement of thermal neutron cross section and resonance integral of the reaction $^{135}\text{Cs} (n, \gamma)$ and ^{136}Cs . *J. Nucl. Sci. Technol.* **1997**, *34*, 431-438.
3. Coughtrey, P. J.; Thorne, M. C. Radionuclide distribution and transport in terrestrial and aquatic ecosystems. A critical review of data. Balkema, A. A., Rotterdam, **1983**; Vol. 3; p 372.
4. Thoraesus, R. Cesium-137 and its gamma radiation in tele radiotherapy. *Acta Radiologica.* **1961**, *55*, 385-395.
5. Banerjee, S.; Mahantshetty, U.; Shrivastava, S. Brachytherapy in India-a long road ahead. *J. Contemp. Brachytherapy.* **2014**, *6*, 331-335.
6. Loftus, T. P. Standardization of cesium-137 gamma-ray sources terms of exposure units (Roentgens). *J. Res. Natl. Bur. Stand. A. Phys. Chem.* **1970**, *74*, 1-2.
7. Fan, Q.; Tanaka, K.; Sakaguchi, A.; Kondo, H.; Watanabe, N. Factors controlling radiocesium distribution in river sediments; field and laboratory studies after the Fukushima Daichi Nuclear Power Plant accidents. *Appl. Geochem.* **2014**, *48*, 93-103.
8. Katz, J. Lessons learned from nonproliferation successes and failures. *Comparative Strategy.* **2008**, *27*, 426-430.
9. Lavoy, P. R Nuclear proliferation over the next decade: causes, warning signs, and policy responses. *Nonproliferation Review.* **2006**, *13*, 434-453.

10. Sources and effects of ionizing radiation: United Nations Scientific Committee on the Effects of Atomic radiation. UNSCEAR 2000 report to the General Assembly, with scientific annexes; *United Nations*, **2000**, pp 2-14.
11. Mizuno, T.; Kubo, H. Overview of active cesium contamination of freshwater fish in Fukushima and eastern Japan. *Scientific Reports*, **2013**, *3*, 1-4.
12. Zalewska, T.; Suplinska, M. Fish pollution with anthropogenic ¹³⁷Cs distribution in the southern Baltic Sea chemosphere. *J. Environ. Radioact.* **2013**, *90*, 1760-1766.
13. Argonne National Laboratory. Human Health Fact Sheet; Cesium, <http://ead.anl.gov/pub/doc/cesium>, **2001**. (accessed July 20, 2017).
14. Harada, K. H.; Fujii, Y.; Adachi, A.; Tsukidate, A.; Asai, F.; Koizumi, A. Dietary intake of radiocesium in dult residents in Fukushima prefecture and neighboring regions after the Fukushima Nuclear Power Plant Accident: 24-h Food-Duplicate Survey in December 2011. *Environ. Sci. Technol.* **2013**, *47*, 2520-2526.
15. Keum, D.-K.; Jun, I.; Lim, K.-M.; Choi, Y.-H. Radiation dose to human and non-human biota in the republic of Korea resulting from the Fukushima Nuclear accident. *Nucl. Eng. Technol.* **2013**, *45*, 1-12.
16. Tronko, M. D.; Bogdanova, T. I.; Komissarenko, I. V.; Epstein, O. V.; Oliynyk, V.; Kovalenko, A.; Likhtarev, I. A.; Kairo, I.; Peters, S. B.; LiVolsi, V. A., Thyroid carcinoma in children and adolescents in Ukraine after the Chernobyl nuclear accident. *Cancer*. **1999**, *86*, 149-156.
17. Collins, B. J.; Chiappetta, G.; Schneider, A. B.; Santoro, M.; Pentimalli, F.; Fogelfeld, L.; Gierlowski, T.; Shore-freedman, E.; Jaffe, G.; Fusco, A. RET expression in papillary thyroid cancer from patients irradiated in childhood for benign conditions. *J. Clin. Endocrinol. Metab.* **2002**, *87*, 3941-3946.

18. Alexakhin, R.; Anspaugh, L.; Balonov, M et al. Environmental consequences of the Chernobyl accident and their remediation: Twenty years of experience. International Atomic Energy Agency; Vienna, Austria, **2006**.
19. Matsunaga, T.; Nagao, S.; Ueno, T.; Takeda, S.; Amano, H.; Tkachenko, Y. Association of dissolved radionuclides released by the Chernobyl accident with colloidal materials in surface water. *Appl. Geochem.* **2004**, *19*, 1581-1599.
20. Mahura, A.; Baklanov, A.; Sørensen, J. H. Long-term probabilistic atmospheric transport and deposition patterns from nuclear risk sites in euro-arctic region. Danish Meteorological Institute Scientific Report: Apatity, Russia, **2003**.
21. Corcho-Alvarado, J. A.; Balsiger, B.; Sahli, H.; Astner, M, Byrde, M. F.; Rollin, S.; Holzer, R.; Mosimann, N.; Wüthrich, S.; Jakob, A.; Burger, M. Long-term behavior of ^{90}Sr and ^{137}Cs in the environment: case studies in Switzerland. *J. Environ. Radioact.* **2016**, *160*, 54-63.
22. Sansone, U.; Belli, M.; Voitsekoitch, O.; Kanivets, V. ^{137}Cs and ^{90}Sr in water and suspended particle matter of the Dnieper river -reservoir system (Ukraine). *Sci. Total Environ.* **1996**, *186*, 257-271.
23. Macdonald, R. W.; Bewers, J. M. Contaminants in the arctic marine environment: priorities for protection. *ICES J. Mar. Sci.* **1996**, *53*, 537-563.
24. Nagao, S.; Kanamori, M.; Ochiai, S.; Tomihara, S.; Fukushi, K.; Yamamoto, M. Export of ^{134}Cs and ^{137}Cs in the Fukushima river systems at heavy rains by typhoon roke in September 2011. *Biogeosci.* **2013**, *10*, 6215-6223.
25. Parajuli, D.; Tanaka, H.; Hakuta, Y.; Minami, K.; Fukuda, S.; Umeoka, K.; Kamimura, R.; Hayashi, Y.; Ouchi, M.; Kawamoto, T. Dealing with the aftermath of Fukushima Daiichi Nuclear accident: decontamination of radioactive cesium enriched ash. *Environ. Sci. Technol.* **2013**, *47*, 3800-3806.

26. Tanaka, K.; Takahashi, Y.; Sakaguchi, A.; Umeo, M.; Hayakawa, S.; Tanida, H.; Saito, T.; Kanai, Y. Vertical profiles of ^{131}I and ^{137}Cs in soils in Fukushima Prefecture related to the Fukushima Daiichi Nuclear Power station accident. *J. Geochem.* **2012**, *46*, 73-76.
27. Chino, M.; Nakayama, H.; Nagai, H.; Terada, H.; Kataka, G.; Yamazawa, H. Preliminary estimation of release amount of ^{131}I and ^{137}Cs accidentally discharged from Fukushima Daichi Nuclear Power Plant into the atmosphere. *J. Nucl. Sci. Technol.* **2011**, *48*, 1129-1134.
28. Mettler, F. A.; Voelz, G. L. Major radiation exposure-what to expect and how to respond. *N. Engl. J. Med.* **2002**, *346*, 1554-1561.
29. Awual, M. R.; Miyazaki, Y.; Taguchi, T.; Shiwaku, H.; Yaita, T. Encapsulation of cesium from contaminated water with highly selective facial organic-inorganic mesoporous hybrid adsorbent. *Chem. Eng. J.* **2016**, *291*, 128-137.
30. Mohapatra, P.; Ansari, S.; Sarkar, A.; Bhattacharyya, A.; Manchanda, V. Evaluation of calix-crown ionophores for selective separation of radio-cesium from acidic nuclear waste solution. *Anal. Chim. Acta.* **2006**, *571*, 308-314.
31. Nabi, S. A.; Naushad, M. Synthesis and characterization of a new inorganic cation-exchanger Zr (IV) tungstomolybdate: Analytical applications for metal content determination in real sample and synthetic mixture. *J. Hazard Mater.* **2007**, *142*, 404-411.
32. Gupta, V.; Singh, P.; Rahman, N. Synthesis, characterization, and analytical application of zirconium (IV) seleniodate, a new cation exchanger. *Anal. Bioanal. Chem.* **2005**, *381*, 471-476.
33. Lujanienė, G.; Motiejūnas, S.; Šapolaitė, J. Sorption of Cs, Pu and Am on clay minerals. *J. Radioanal. Nucl. Chem.* **2007**, *274*, 345-353.

34. Weiss, C. A.; Kirkpatrick, R. J.; Altaner, S. P. The structural environments of cations adsorbed onto clays: ^{133}Cs variable-temperature MAS NMR spectroscopic study of hectorite. *Geochim. Cosmochim. Acta.* **1990**, *54*, 1655-1669.
35. Rani, R. D.; Sasidhar, P. Sorption of cesium on clay colloids: kinetic and thermodynamic studies. *Aquat. Geochem.* **2012**, *18*, 281-296.
36. Du, Z.; Jia, M.; Wang X. Cesium removal from solution using pan-based potassium nickel hexacyanoferrate (II) composite spheres. *J. Radioanal. Nucl. Chem.* **2013**, *298*, 167-177.
37. Han, F.; Guang-Hui, Z.; Gu, P. Removal of cesium from simulated liquid waste with countercurrent two-stage adsorption followed by microfiltration. *J. Hazard Mater.* **2012**, *225*, 107-110.
38. Kamaraj, R.; Vasudevan, S. Evaluation of electrocoagulation process for the removal of strontium and cesium from aqueous solution. *Chem. Eng. Res. Des.* **2015**, *93*, 522-530.
39. Darder, M.; Gonzalez-Alfaro, Y.; Aranda, P.; Ruiz-Hitzky, E. Silicate-based multifunctional nanostructured materials with magnetite and prussian blue: application to cesium uptake. *RSC. Adv.* **2014**, *4*, 35415-35421.
40. Olatunji, M. A.; Khandaker, M. U.; Mahmud, H. N. M. E.; Amin, Y. M. Influence of adsorption parameters on cesium uptake from aqueous solutions-a brief review. *RSC Adv.* **2015**, *5*, 71658-71683.
41. Kozhevnikov, I. V. Catalysis by heteropoly acids and multicomponent polyoxometalates in liquid-phase reactions. *Chem. Rev.* **1998**, *98*, 171-198.
42. Newman, A. D.; Lee, A. F.; Wilson, K.; Young, N. A. On the active site in the $\text{H}_3\text{W}_{12}\text{O}_{40}/\text{SiO}_2$ catalysts for fine chemical synthesis. *Catal. Lett.* **2005**, *102*, 45-50.

43. Okuhara, T.; Watanabe, H.; Nishimura, T.; Inumaru, K.; Misono, M. Microstructure of cesium hydrogen salts of 12-tungstophosphoric acid relevant to novel acid catalysis. *Chem. Mater.* **2000**, *12*, 2230-2245.
44. Kozhevnikov, I. V. Advances in catalysis by heteropoly acids. *Chem. Rev.* **1997**, *56*, 811-813.
45. Mizuno N.; Misono, M. Heterogeneous catalysis. *Chem. Rev.* **1998**, *98*, 199-217.
46. Yang, L.; Qi, Y.; Yuan X.; Shen, J.; Kim, J. Direct synthesis, characterization and catalytic application of SBA-15 containing heteropolyacid H₃PW₁₂O₄₀. *J. Mol. Catal. A-Chem.* **2005**, *229*, 199-205.
47. Rafiee, E.; Rashidzadeh, S.; Azad, A. Silica-supported heteropoly acids: highly efficient catalysts for synthesis of aminonitriles, using trimethylsilyl cyanide or potassium cyanide. *J. Mol. Catal. A-Chem.* **2007**, *261*, 49-52.
48. Borai, E. H.; Harjula, R.; Malinen, L.; Paajanen, A. Efficient removal of cesium from low-level radioactive liquid waste using natural and impregnated zeolite minerals. *J. Hazard Mater.* **2009**, *172*, 416-422.
49. Aany Sofia, L. T.; Krishnan, A.; Sankar, M.; Kaj, N. K. K.; Manikadan, P.; Rajamohanam, P. R.; Ajithkumar, T. G. Immobilization of phosphotungstic acid (PTA) on imidazole functionalized silica; evidence for the nature of PTA binding by solid state NMR and reaction studies. *J. Phys. Chem.* **2009**, *113*, 21114-21122.
50. Hoo, P. Y.; Abdullah, A. Z. Direct synthesis of mesoporous 12-tungstophosphoric acid SBA-15 catalyst for selective esterification of glycerol and lauric acid to monolaurate. *Chem. Eng. J.* **2014**, *250*, 274-287.
51. Kaleta, W.; Nowinska, K. Immobilisation of heteropoly anions in Si-MCM-41 channels by means of chemical bonding to aminosilane groups. *Chem. Commun.* **2001**, *535*, 41-50.

52. Seaton, K.; Little, I.; Tate, C.; Mohseni, R.; Roginskaya, M.; Povazhniy, V.; Vasiliev, A. Adsorption of cesium on silica gel containing embedded phosphotungstic acid. *Microporous Mesoporous Mater.* **2017**, *244*, 55-66.
53. Adetola, O.; Golovko, L.; Vasiliev, A. Modification of silica gel by heteropolyacids. *Key Eng. Mater.* **2016**, *689*, 126-132.
54. Little, I.; Seaton, K.; Alorkpa, E.; Vasiliev, A. Adsorption of cesium on bound porous materials containing embedded phosphotungstic acid. *Adsorption.* **2017**, *23*, 809-819.
55. Little, I.; Alorkpa, E.; Khan, V.; Povazhny, V.; Vasiliev, A. Efficient porous adsorbent for removal of cesium from contaminated. *J. Porous Mater.* **2019**, <https://doi.org/10.1007/s10934-018-0608-1>
56. Edwards, J. C.; Thiel, C. Y.; Benac, B.; Knifton, J. F. Solid-state NMR and FT-IR investigation of 12-tungstophosphoric acid on TiO₂. *Catal. Lett.* **1998**, *51*, 77-83.
57. Haouas, M.; Taulelle, F.; Martineau, C. Recent advances in application of ²⁷Al NMR spectroscopy to materials Science. *Prog. Nucl. Magn. Reson. Spectrosc.* **2016**, *94-95*, 11-36.
58. Samain, L.; Jaworski, A.; Edén, M.; Ladd, D. M.; Seo, D. K.; Garcia-Garcia, F.J.; Häussermann, U. Structural analysis of highly porous γ -Al₂O₃. *J. Solid State Chem.* **2014**, *217*, 1-8.
59. Chen, L.; Bai, B. Facile Preparation of Phosphotungstic Acid-Impregnated Yeast Hybrid Microspheres and Their Photocatalytic Performance for Decolorization of Azo Dye. *Int. J. Photoenergy.* **2013**, ID: 406158. <https://dx.doi.org/10.1155/2013/406158>
60. Marosi, L.; Platero, E. E.; Cifre, J.; Arean, C. O. Thermal dehydration of H_{3+x}PV_xM_{12-x}O₄₀·yH₂O Keggin type heteropolyacids; formation, thermal stability and structure of the anhydrous acids H₃PM₁₂O₄₀ of the corresponding anhydrides

- PM₁₂O_{38.5} and of a novel trihydrate H₃PW₁₂O₄₀·3H₂O. *J. Mater. Chem.* **2000**, *10*, 1949-1955.
61. Müller, P.; Seeger, M.; Tomas, J. Compression and breakage behaviour of γ -Al₂O₃ granules. *Powder Technol.* **2013**, *237*, 125-133.
62. Caliman, E.; Dias, J. A.; Dias, S. C. L.; Prado, A.G.S. Solvent effect on the preparation of H₃PW₁₂O₄₀ supported on alumina. *Catal. Today.* **2005**, *107-108*, 816-825.
63. Okuhara, T.; Tatematsu, S.; Lee, K. Y.; Misoni, M. Catalysis by heteropoly compounds. XII. Absorption properties of 12-tungstophosphoric acid and its salts. *Bull. Chem. Soc. Jpn.* **1989**, *62*, 717-723.
64. Banerjee, S.; Kar, K. K. Aluminum-substituted phosphotungstic acid/sulfonated polyether ketone nanocomposite membrane with reduced leaching and improved proton conductivity. *High Perform. Polym.* **2016**, *28*, 1043-1058.
65. Rao, M. K.; Gobetto, R.; Iannibello, A.; Zecchina, A. Solid state NMR and IR studies of phosphomolybdenum and phosphotungsten heteropoly acids supported on SiO₂, γ -Al₂O₃, and SiO₂-Al₂O₃. *J. Catal.* **1989**, *119*, 512-516.
66. Zhu, Z.; Tain, R.; Rhodes, C. A study of the decomposition behaviour of 12-tungstophosphate heteropolyacid in solution. *Can. J. Chem.* **2003**, *81*, 1044-1050.

VITA

ESTHER ALORKPA

- Education: M.S. East Tennessee State University, Johnson City, TN (May 2019)
- B.S. University of Science and Technology, Kumasi, Ghana (May 2016)
- Professional Experience: Laboratory Assistant, Chemistry Department, Ghana Standards Authority (GSA), Accra, Ghana (June 2012 – July 2016)
- Teaching: Teaching Assistant, Chemistry Department, East Tennessee State University (January 2017 – December 2018)
- University of Science and Technology, Ghana (August 2016 – August 2018) Teaching/Research Assistant
- Chemistry Instructor, East Tennessee State University Upward Bound Program
- Publications: Little, I.; Seaton, K.; Alorkpa, E.; Vasiliev, A. Adsorption of cesium on bound porous materials containing embedded phosphotungstic acid. *Adsorption*. **2017**, *23*, 809-819
- Little, I.; Alorkpa, E.; Khan, V.; Povazhny, V.; Vasiliev, A. Efficient porous adsorbent for removal of cesium from contaminated. *J. Porous Mater.* **2019**, <https://doi.org/10.1007/s10934-018-0608-1>

Alorkpa, E.; Boadi, N. O.; Badu M.; Saah, S. A. Phytochemical screening, antimicrobial, antioxidant properties of assorted carica papaya in Ghana. *J. Med. Plants Stud.* **2016**, *4*, 193-198.